

Accelerated PDE's for efficient solution of regularized inversion problems

Minas Benyamin* Jeff Calder† Ganesh Sundaramoorthi‡
 Anthony Yezzi§

October 2, 2018

Abstract

We further develop a new framework, called *PDE Acceleration*, by applying it to calculus of variations problems defined for general functions on \mathbb{R}^n , obtaining efficient numerical algorithms to solve the resulting class of optimization problems based on simple discretizations of their corresponding accelerated PDE's. While the resulting family of PDE's and numerical schemes are quite general, we give special attention to their application for regularized inversion problems, with particular illustrative examples on some popular image processing applications. The method is a generalization of momentum, or accelerated, gradient descent to the PDE setting. For elliptic problems, the descent equations are a nonlinear damped wave equation, instead of a diffusion equation, and the acceleration is realized as an improvement in the CFL condition from $\Delta t \sim \Delta x^2$ (for diffusion) to $\Delta t \sim \Delta x$ (for wave equations). We work out several explicit as well as a semi-implicit numerical schemes, together with their necessary stability constraints, and include recursive update formulations which allow minimal-effort adaptation of existing gradient descent PDE codes into the accelerated PDE framework. We explore these schemes more carefully for a broad class of regularized inversion applications, with special attention to quadratic, Beltrami, and Total Variation regularization, where the accelerated PDE takes the form of a nonlinear wave equation. Experimental examples demonstrate the application of these schemes for image denoising, deblurring, and inpainting, including comparisons against Primal Dual, Split Bregman, and ADMM algorithms.

*School of Electrical and Computer Engineering, Georgia Institute of Technology.
 (minasbenyamin@gatech.edu)

†School of Mathematics, University of Minnesota. (jcalder@umn.edu)

‡United Technologies Research Center, East Hartford, CT (ganesh.sun@gmail.com)

§School of Electrical and Computer Engineering, Georgia Institute of Technology.
 (anthony.yezzi@ece.gatech.edu)

1 Introduction

Variational problems have found great success, and are widely used, in image processing for problems such as noisy or blurry image restoration, image inpainting, image decomposition, and many other problems [2]. Many image processing problems have the form

$$(1) \quad \min_u \int_{\Omega} L(x, u, \nabla u) dx$$

where L is convex in ∇u ¹ and the corresponding gradient descent equation

$$u_t + L_z(x, u, \nabla u) - \operatorname{div}(\nabla_p L(x, u, \nabla u)) = 0$$

is a nonlinear diffusion equation, where $L = L(x, z, p)$. Solving (1) via gradient descent is inefficient, due in large part to the stiff stability (CFL) condition $\Delta t \leq C\Delta x^2$ for diffusion equations. This has led to the development of more efficient optimization algorithms, such as primal dual methods [7] and the split Bregman approach [9] that avoid this numerical stiffness.²

Optimization is also widely used in machine learning, though the types of optimization problems are (usually) structurally different than in image processing. As in image processing, for modern large scale problems in machine learning first order methods based on computing only the gradient are preferable, since computing and storing the Hessian is intractable [4]. The discrete version of gradient descent is

$$(2) \quad x_{k+1} = x_k - \alpha \nabla f(x_k),$$

where in machine learning the time step α is called the *learning rate*. While gradient descent is provably convergent for convex problems [5], the method can be very slow to converge in practice.

To address this issue, many versions of *accelerated* gradient descent have been proposed in the literature, and are widely used in machine learning [25]. At some heuristic level, gradient descent is often slow to converge because the local descent direction is not reliable on a larger scale, leading to large steps in poor directions and large corrections in the opposite direction. Accelerated descent methods incorporate some type of averaging of past descent directions, which provides a superior descent direction compared to the local gradient. One of the oldest accelerated methods is Polyak's heavy ball method [16]

$$(3) \quad x_{k+1} = x_k - \alpha \nabla f(x_k) + \beta(x_k - x_{k-1}).$$

The term $\beta(x_k - x_{k-1})$ acts to average the local descent direction with the previous direction, and is referred to as *momentum*. Polyak's heavy ball method was studied in the continuum by Attouch, Goudou, and Redont [1], and also by Goudou and Munier [10], who call it the

¹Nonconvex problems are also widely used, see e.g., [15].

²Primal dual and split Bregman also avoid the non-smoothness of the L^1 norm, which is an issue in descent based approaches, which require some regularization.

heavy ball with friction. In the continuum, Polyak’s heavy ball method corresponds to the equations of motion for a body in a potential field, which is the second order ODE

$$(4) \quad \ddot{x} + a\dot{x} = -\nabla f(x).$$

A more recent example of momentum descent is the famous Nesterov accelerated gradient descent [14]

$$(5) \quad x_{k+1} = y_k - \alpha \nabla f(y_k), \quad y_{k+1} = x_{k+1} + \frac{k-1}{k+2}(x_{k+1} - x_k).$$

In [14] Nesterov proved a convergence rate of $O(1/t^2)$ after t steps for strongly convex problems. This is provably optimal for first order methods.

The seminal works of Polyak and Nesterov have spawned a whole field of momentum-based descent methods, and variants of these methods are widely used in machine learning, such as the training of neural networks in deep learning [22,25]. The methods are popular for both their superior convergence rates for convex problems, but also their ability to avoid local minima in nonconvex problems, which is not fully understood in a rigorous sense. There has been significant interest recently in understanding the Nesterov accelerated descent methods. In particular, Su, Boyd and Candes [19] recently showed that Nesterov acceleration is simply a discretization of the second order ODE

$$(6) \quad \ddot{x} + \frac{3}{t}\dot{x} = -\nabla f(x).$$

Other works have since termed this ODE as *continuous time Nesterov* [23]. We note the friction coefficient $3/t$ vanishes as $t \rightarrow \infty$, which explains why many implementations of Nesterov acceleration involve *restarting*, or resetting the time to $t = 0$ when the system is underdamped [23].

However, it is the work of Wibisono, Wilson, and Jordan [25] that gives the clearest picture of Nesterov acceleration. They show that virtually all Nesterov accelerated gradient descent methods are simply discretizations of the ODE equations of motion for a particular Lagrangian action functional. This endows Nesterov acceleration with a variational framework, which aids in our understanding, and more importantly can be easily adapted to other settings.

This was extended to the partial differential equation (PDE) setting by Sundaramoorthi and Yezzi in two initial works [20,26] (see also [21]) where the first set of *Accelerated PDE’s* were formulated both for geometric flows of contours and surfaces (active contours) as well as for diffeomorphic mappings between images (optical flow). There are also some acceleration-type methods that have appeared recently in image processing [3, 11, 12, 24], however these methods are not derived from a variational framework, and so they lack energy monotonicity and convergence guarantees.

1.1 Contributions and Outline of Paper

In this paper, we extend the class of *Accelerated PDE’s* formulated in [20,26] to the setting of generic functions over \mathbb{R}^n , building on the variational insights pioneered by [25]. The

method applies to solving general problems in the calculus of variations. In similar spirit to (4) and (6), the descent equations in PDE acceleration correspond to a continuous second order flow in time which, for a broad class of regularized inversion problems to be addressed in Section 4, take on the specific form of damped nonlinear *wave* equations rather than the reaction-diffusion equations that arise as their traditional gradient descent counterparts. Accelerated PDE's can be solved numerically with simple explicit Euler or semi-implicit Euler schemes which we develop in Section 3. Here, acceleration is realized in part through an improvement in the CFL condition from $\Delta t \sim \Delta x^2$ for diffusion equations (or standard gradient descent), to $\Delta t \sim \Delta x$ for wave equations. In fact, we will show early on in Section 3 that the improvement in the CFL condition for explicit numerical accelerated PDE schemes (compared with their gradient descent counterparts) is a completely general property of accelerated PDE's which applies even when the wave equation structure explored with more detail in Section 4 does not arise.

In Section 5 we apply the method to quadratic, Beltrami, and Total Variation regularized problems in image processing including denoising, deblurring, and inpainting, obtaining results that are comparable to state of the art methods, such as the split Bregman approach, and ADMM, and superior to primal dual methods. In a companion paper [6] we study the PDE acceleration method rigorously and prove a convergence rate, perform a complexity analysis, and show how to optimally select the parameters, including the damping coefficient (these results are summarized in Section 2).

1.2 Acknowledgments

Jeff Calder was supported by NSF-DMS grant 1713691.

Anthony Yezzi was supported by NSF-CCF grant 1526848 and ARO W911NF-18-1-0281.

2 PDE acceleration

We now present our PDE acceleration framework, which is based on the seminal work of [20,25,26] with suitable modifications to image processing problems. We consider the calculus of variations problem

$$\min_u E[u] := \int_{\Omega} \Phi(x, \nabla u) + \Psi(x, u) dx.$$

The Euler-Lagrange equation satisfied by minimizers is

$$(7) \quad \nabla E[u] := \Psi_z(x, u) - \operatorname{div}(\nabla \Psi(x, \nabla u)) = 0,$$

where $\Phi = \Phi(x, p)$, $\nabla \Phi = \nabla_p \Phi$ and $\Psi = \Psi(x, z)$. We note that the gradient $\nabla E[u]$ satisfies

$$(8) \quad \left. \frac{d}{d\varepsilon} \right|_{\varepsilon=0} E[u + \varepsilon v] = \int_{\Omega} \nabla E[u] v dx$$

for all v smooth with compact support, and is often called the L^2 -gradient due to the presence of the L^2 inner product on the right hand side.

We define the action integral

$$(9) \quad J[u] = \int_{t_0}^{t_1} k(t) \left(\frac{1}{2} \int_{\Omega} \rho u_t^2 dx - b(t)E[u] \right) dt,$$

where $k(t)$ and $b(t)$ are time dependent weights, $\rho = \rho(x)$ represents a mass density, and $u = u(x, t)$. Notice the action integral is the weighted difference between kinetic energy $\frac{1}{2} \int \rho u_t^2 dx$ and potential energy $E[u]$. The PDE accelerated descent equations are defined to be the equations of motion in the Lagrangian sense corresponding to the action J . To compute the equations of motion, we take a variation on J to obtain

$$0 = \left. \frac{d}{d\varepsilon} \right|_{\varepsilon=0} J[u + \varepsilon v] = \int_{t_0}^{t_1} \int_{\Omega} k(t) \rho u_t v_t - k(t) b(t) \nabla E[u] v dx$$

for smooth v with compact support in $\Omega \times (t_0, t_1)$. Integrating by parts in t we have

$$0 = \int_{t_0}^{t_1} \int_{\Omega} \left[-\frac{\partial}{\partial t} (k(t) \rho u_t) - k(t) b(t) \nabla E[u] \right] v dx.$$

Therefore, the PDE accelerated descent equations are

$$\frac{\partial}{\partial t} (k(t) \rho u_t) = -k(t) b(t) \nabla E[u].$$

It is more convenient to define $a(t) = k'(t)/k(t)$ are rewrite the descent equations as

$$(10) \quad \boxed{u_{tt} + a(t)u_t = -b(t)\rho(x)^{-1}\nabla E[u].}$$

For image processing problems, there is typically no Dirichlet boundary condition, so the natural variational boundary condition $\nabla_p \Phi(x, \nabla u) \cdot \mathbf{n} = 0$ is imposed on the boundary $\partial\Omega$, where \mathbf{n} is the outward normal. Often this reduces to the Neumann condition $\frac{\partial u}{\partial \mathbf{n}} = 0$.

In a companion paper [6] we study the PDE acceleration descent equation (10) rigorously. In particular, we prove energy monotonicity, and a linear convergence rate. We summarize the results in Lemma 1 and Theorem 1.

Lemma 1 (Energy monotonicity [6]). *Assume $a(t), b(t) \geq 0$ and let u satisfy (10). Suppose either $u(x, t) = g(x)$ or $\nabla \Phi(x, \nabla u) \cdot \mathbf{n} = 0$ on $\partial\Omega$. Then*

$$(11) \quad \frac{d}{dt} (K[u] + b(t)E[u]) = -2a(t)K[u] + b'(t)E[u],$$

where $K[u] = \frac{1}{2} \int_{\Omega} \rho u_t^2 dx$. In particular, total energy is always decreasing provided $b'(t) \leq 0$ and $E[u] \geq 0$.

Theorem 1 (Convergence rate [6]). *Let u satisfy (10) and let u^* be a solution of $\nabla E[u^*] = 0$ in Ω . Assume Φ is uniformly convex in ∇u , Ψ is convex, and Ψ_{zz} is bounded above, $u = u^*$ on $\partial\Omega$, $a(t) = a > 0$ is constant and $b(t) \equiv 1$ and $\rho \equiv 1$. Then there exists $C, \beta > 0$ such that*

$$(12) \quad \|u - u^*\|_{H^1(\Omega)}^2 \leq C \exp(-\beta t).$$

We mention that the same convergence rate (12) holds for gradient descent

$$u_t = -\nabla E[u]$$

under the same conditions on E . The difference is that gradient descent is a diffusion equation, which requires a time step of $\Delta t \sim \Delta x^2$ for stability, while PDE acceleration (10) is a wave equation which allows much larger time steps $\Delta t \sim \Delta x$. Thus, the acceleration is realized as a relaxation in the CFL condition.

While Theorem 1 provides a convergence rate, it does not give advice on how to select the damping coefficient $a > 0$. It was shown in [6] how to optimally select the damping coefficient in the linear setting, and we find this choice is useful for nonlinear problems as well. For convenience, we recall the results from [6], which apply to the linear PDE acceleration equation

$$(13) \quad u_{tt} + au_t + Lu + \lambda u = f \quad \text{in } \Omega \times (0, \infty),$$

where L is a linear second order elliptic operator. A Fourier analysis [6] leads to the optimal choice

$$(14) \quad a = 2\sqrt{\lambda_1 + \lambda},$$

where λ_1 is the first Dirichlet eigenvalue of L (or for the Neumann problem, the first eigenvalue corresponding to a nontrivial eigenfunction), and the optimal convergence rate

$$(15) \quad |u(x, t) - u^*(x)| \leq C \exp(-at).$$

Notice that if L is degenerate elliptic, so $\lambda_1 = 0$, which roughly corresponds to a non-strongly convex optimization problem, the method still converges when $\lambda > 0$. That is, the presence of a fidelity term in the image processing problem enables, and accelerates, convergence. This suggests why the algorithm is successful even for TV restoration, which is not strongly convex but has a fidelity.

3 Numerical Schemes for Accelerated PDE's

We now describe various time discretization strategies for the generic accelerated PDE

$$(16) \quad u_{tt} + au_t = -\nabla E[u, u_x, u_{xx}, \dots] \quad \text{accelerated PDE}$$

$$(17) \quad u_t = -\nabla E[u, u_x, u_{xx}, \dots] \quad \text{gradient descent PDE}$$

(alongside related discretizations of the generic gradient descent PDE for comparison) where (16) represents the unit density ($\rho = 1$) and unit energy scaled ($b = 1$) case of (10). A key advantage of accelerated PDE schemes for regularized inversion problems, which we explore subsequently in Section 4, is that in typical cases where the gradient descent PDE (17) takes the form of a linear or nonlinear reaction-diffusion equation, the matching accelerated PDE (16) takes the form of a linear or nonlinear wave equation, whose explicit time discretization permits a much larger stable time step than the explicit discretization of (17). Therefore, due to their simplicity of implementation, as well as their immediately parallelizable structure, we will restrict our discussion to explicit update schemes and to the semi-implicit Euler scheme whose two-part update consists of partial updates which are both explicit in nature.

3.1 Explicit Forward-Euler for Gradient Descent PDE's

We start by considering the explicit forward Euler discretization of the continuous gradient descent PDE (17). Using a forward difference in time to approximate the time derivative on the left hand side we obtain

$$\frac{u(x, t + \Delta t) - u(x, t)}{\Delta t} = -\nabla E$$

This leads to the following simple discrete iteration

$$(18) \quad \begin{aligned} \Delta u^n(x) &= -\Delta t \nabla E^n \\ u^{n+1}(x) &= u^n(x) + \Delta u^n(x) \end{aligned}$$

where $u^n(x) \doteq u(x, n\Delta t)$ denotes the current iterate, $\Delta u^n \doteq u(x, n\Delta t + \Delta t) - u(x, n\Delta t)$ the increment to be applied, $u^{n+1}(x) \doteq u(x, (n+1)\Delta t)$ the new iterate, and $\nabla E^n(x) \doteq \nabla E(x, n\Delta t)$ the discrete approximation of the gradient computed at step n .

In most cases, stability considerations require an upper bound on the time step Δt (the CFL condition) dependent upon the discretization of ∇E^n . Often this upper bound for stable time steps is computed using Von Neumann analysis by linearizing ∇E^n in (18) and taking a Discrete Fourier Transform (DFT) on both sides of the homogeneous part to obtain.

$$U^{n+1}(\omega) - U^n(\omega) = -\Delta t [z(\omega)U^n(\omega)]$$

Such a structure often arises when ∇E^n is computed explicitly using only the values of u^n . In such cases, its linearization will consist of a combination of u^n values whose DFT can be written in the form $z(\omega)U^n(\omega)$ where $U^n(\omega)$ denotes the DFT of u^n . We will refer to $z(\omega)$ as the *gradient amplifier*.³

This leads to the following update

$$(19) \quad \begin{aligned} U^{n+1}(\omega) &= \underbrace{(1 - \Delta t z(\omega))}_{\xi(\omega)} U^n(\omega) \\ \text{gradient amplifier } z(\omega) &\doteq \frac{\text{DFT}(\text{linearized_homogeneous_part_of}(\nabla E^n))}{\text{DFT}(u^n)} \end{aligned}$$

³ A discrete version of what is often called the *symbol* of the underlying linear differential operator that is being approximated.

which will be stable as long as the overall update amplification factor $\xi(\omega)$ does not have complex amplitude exceeding unity for any frequency ω . This condition can be expressed as

$$\begin{aligned}\xi(\omega)\xi^*(\omega) &= (1 - \Delta t z(\omega))(1 - \Delta t z^*(\omega)) \leq 1 \\ \Delta t &\leq \frac{z(\omega) + z^*(\omega)}{z(\omega)z^*(\omega)} = \frac{1}{z(\omega)} + \frac{1}{z^*(\omega)} = 2\Re\left(\frac{1}{z(\omega)}\right)\end{aligned}$$

For elliptic operators, which are common in regularized optimization in image processing, the gradient amplifier is real and non-negative: $z(\omega) \geq 0$. In such cases the stability constraint takes the form of the following CFL condition

$$(20) \quad \Delta t \leq \frac{2}{z_{\max}}$$

where $z_{\max} \doteq \max_{\omega} z(\omega)$.

3.2 Fully Explicit Schemes for Accelerated PDE's

We now turn our attention to the explicit discretizations of the accelerated PDE (16). We will consider both first and second order approximations of the time derivatives and will exploit the following lemma in the Von Neumann stability analysis for each of these choices.

Root Amplitude Lemma *Given a quadratic equation $A\xi^2 + B\xi + C = 0$ with real coefficients ($A \neq 0$), its roots will satisfy $|\xi| \leq 1$ if and only if $\frac{|B|}{|A|} - 1 \leq \frac{C}{A} \leq 1$ (or equivalently $A > C$ and $A + C > |B|$ for positive A).*

Proof. We first prove the result in the special case that $A = 1$ and $B \geq 0$, in which case the roots are $\xi = -\frac{B}{2} \pm \frac{1}{2}\sqrt{B^2 - 4C}$ and claim that $|\xi| \leq 1$ if and only if

$$B - 1 \leq C \leq 1$$

If the roots are imaginary, then both have complex amplitude $|\xi|^2 = C > 0$ which makes the right hypothesis both necessary and sufficient. The left hypothesis automatically follows since $C > \frac{B^2}{4} \geq B - 1$ (the first part for the roots to be imaginary and the second part equivalent to $(B - 2)^2 \geq 0$). In the case of real roots, we want the larger magnitude root to satisfy $|\xi| = \frac{B}{2} + \frac{1}{2}\sqrt{B^2 - 4C} \leq 1$, which can be expressed as $\sqrt{B^2 - 4C} \leq 2 - B$. This immediately yields $B \leq 2$ as a necessary condition to keep the right side positive. Under this condition, we can square both sides and simplify to obtain the left hypothesis as necessary and sufficient. The right hypothesis automatically follows since $C < \frac{B^2}{4} < 1$ (the first part for the roots to be real and the second part based on our condition). Combining the hypotheses yields $B - 1 \leq 1$ which satisfies the necessary condition, thus completing the special case proof. The general case follows since the roots of $A\xi^2 + B\xi + C$ have the same magnitude as the roots of $\xi^2 + \frac{|B|}{|A|}\xi + \frac{C}{A}$.

3.2.1 Second order in time scheme

Using central difference approximations for both time derivatives gives a second order discretization in time

$$\frac{u(x, t + \Delta t) - 2u(x, t) + u(x, t - \Delta t)}{\Delta t^2} + a \frac{u(x, t + \Delta t) - u(x, t - \Delta t)}{2\Delta t} = -\nabla E(x, t)$$

which leads to the following update.

$$(21) \quad u^{n+1}(x) = \frac{2u^n(x) - \left(1 - \frac{a\Delta t}{2}\right) u^{n-1}(x) - \Delta t^2 \nabla E^n(x)}{1 + \frac{a\Delta t}{2}}$$

Applying the DFT to the linearized homogeneous part of the update scheme (21) yields

$$U^{n+1}(\omega) = \frac{(2 - \Delta t^2 z(\omega)) U^n(\omega) - \left(1 - \frac{a\Delta t}{2}\right) U^{n-1}(\omega)}{1 + \frac{a\Delta t}{2}}$$

where $z(\omega)$ denotes the gradient amplifier (19). If we substitute $U^{n\pm m} = \xi^{\pm m} U^n$, where $\xi(\omega)$ denotes the overall update amplification factor, then we obtain the quadratic equation

$$\underbrace{\left(1 + \frac{a\Delta t}{2}\right)}_A \xi^2 + \underbrace{(\Delta t^2 z(\omega) - 2)}_B \xi + \underbrace{\left(1 - \frac{a\Delta t}{2}\right)}_C = 0$$

In the case of real $z(\omega)$, we may exploit the Root Amplitude Lemma to check the stability condition $|\xi(\omega)| \leq 1$. The first condition $A \geq C$ of the lemma (for positive A) is satisfied since $1 + \frac{a\Delta t}{2} \geq 1 - \frac{a\Delta t}{2}$ for all positive a and Δt , and so we use the second condition $A + C \geq |B|$ to obtain the stability condition $2 \geq |2 - \Delta t^2 z(\omega)|$, which may be rewritten as $0 \leq \Delta t^2 z(\omega) \leq 4$. In the case where $z(\omega) \geq 0$ we automatically satisfy the left hand inequality for all ω , leaving us with

$$(22) \quad \Delta t \leq \frac{2}{\sqrt{z_{\max}}}$$

3.2.2 First order in time schemes

Continuing to use a central difference for the second derivative but only a one sided difference (forward or backward) for the first derivative in time, yields two alternative first order time schemes.

Forward difference

$$\frac{u(x, t + \Delta t) - 2u(x, t) + u(x, t - \Delta t)}{\Delta t^2} + a \frac{u(x, t + \Delta t) - u(x, t)}{\Delta t} = -\nabla E(x, t)$$

The forward difference discretization yields the update.

$$(23) \quad u^{n+1}(x) = \frac{(2 + a\Delta t) u^n(x) - u^{n-1}(x) - \Delta t^2 \nabla E^n(x)}{1 + a\Delta t}$$

Von Neumann analysis applied to the linearized homogeneous part of (21) yields the following quadratic equation for the update amplification factor $\xi(\omega)$.

$$\underbrace{(1 + a\Delta t)}_A \xi^2(\omega) + \underbrace{(\Delta t^2 z(\omega) - 2 - a\Delta t)}_B \xi(\omega) + \underbrace{1}_C = 0$$

Since $1 + a\Delta t > 1$ for all positive a and Δt , the first condition $A \geq C$ of the root amplitude lemma (for positive A) is always satisfied. We may therefore restrict our attention to the second condition $A + C \geq |B|$, assuming real $z(\omega)$, to determine whether $|\xi(\omega)| \leq 1$. This gives the condition $(1 + a\Delta t) + 1 \geq |\Delta t^2 z(\omega) - (2 + a\Delta t)|$ which is equivalent to $0 \leq \Delta t^2 z(\omega) \leq 2(2 + a\Delta t)$. In the case where $z(\omega) \geq 0$ we automatically satisfy the left hand inequality for all ω , which leaves us with $z(\omega) \Delta t^2 - 2a\Delta t - 4 \leq 0$. Plugging in the extreme case z_{\max} and restricting Δt to lie below the positive root in order to keep the quadratic expression on the left negative yields

$$(24) \quad \Delta t \leq \sqrt{\frac{4}{z_{\max}} + \left(\frac{a}{z_{\max}}\right)^2} + \frac{a}{z_{\max}}$$

Notice that the CFL condition (22) for the second order (central difference) scheme is sufficient but not necessary. If, however, we wish to obtain a condition independent of the damping a , then minimizing the upper bound with respect to a (by plugging in $a = 0$) recovers this prior second order CFL condition.

Backward difference

$$\frac{u(x, t + \Delta t) - 2u(x, t) + u(x, t - \Delta t)}{\Delta t^2} + a \frac{u(x, t) - u(x, t - \Delta t)}{\Delta t} = -\nabla E(x, t)$$

The backward difference discretization yields the update.

$$(25) \quad u^{n+1}(x) = (2 - a\Delta t) u^n(x) - (1 - a\Delta t) u^{n-1}(x) - \Delta t^2 \nabla E^n(x)$$

Similar analysis yields the following quadratic equation for the amplification factor $\xi(\omega)$.

$$\xi^2(\omega) - (2 - a\Delta t - \Delta t^2 z(\omega)) \xi(\omega) + (1 - a\Delta t) = 0$$

The first condition $A \geq C$ of the lemma (for positive A) is always satisfied ($1 \geq 1 - a\Delta t$) for all positive values of a and Δt . The second condition $A + C \geq |B|$, assuming real $z(\omega) \geq 0$, of the lemma, can be expressed as $\Delta t^2 z(\omega) + 2a\Delta t - 4 \leq 0$. Plugging in the extreme case z_{\max}

and restricting Δt to lie below the positive root in order to keep the quadratic expression on the left negative gives the following CFL condition.

$$(26) \quad \Delta t \leq \sqrt{\frac{4}{z_{\max}} + \left(\frac{a}{z_{\max}}\right)^2} - \frac{a}{z_{\max}}$$

Notice that the CFL condition (22) for the central difference scheme is necessary (easily seen by applying the triangle inequality) but no longer sufficient as in the forward difference case. Furthermore, the constraint becomes increasingly restrictive as the damping coefficient a increases, making it impossible to formulate a sufficient damping-independent stability constraint. We will therefore give no further consideration to this scheme.

3.3 Recursive Increments and Properties of Explicit Schemes

For greater convenience in implementation, especially when upgrading existing gradient descent routines structured according to (18) with one array to store the evolving iterate u^n and another for its increment Δu^n , the explicit accelerated PDE discretizations can be expressed in terms of recursively defined increments as follows⁴

(27)

$$\text{gradient descent: } \Delta u^n = -\Delta t \nabla E^n, \quad \Delta t \leq \frac{2}{z_{\max}}$$

(28)

$$\text{1-order accelerated: } \Delta u^n = \frac{1}{1+a\Delta t} \Delta u^{n-1} - \frac{\Delta t^2}{1+a\Delta t} \nabla E^n, \quad \Delta t \leq \sqrt{\frac{4}{z_{\max}} + \left(\frac{a}{z_{\max}}\right)^2} + \frac{a}{z_{\max}}$$

(29)

$$\text{2-order accelerated: } \Delta u^n = \frac{2-a\Delta t}{2+a\Delta t} \Delta u^{n-1} - \frac{2\Delta t^2}{2+a\Delta t} \nabla E^n, \quad \Delta t \leq \frac{2}{\sqrt{z_{\max}}}$$

where Δu^{n-1} denotes the previously increment (kept in just one more added array). Here we see more directly the traditional momentum style structure (i.e. heavy-ball) in that the next increment Δu^n is expressed as a weighted combination of the gradient ∇E^n and the previous increment Δu^{n-1} . Recursion (28) is equivalent to the first order in time, explicit update (23) using forward differences while the recursion (29) is equivalent to the second order in time, explicit update (21) using central differences, and as such they must adhere to the same CFL conditions (24) and (22) derived earlier for these corresponding schemes.

⁴For completeness, the first order backward difference scheme can also be written recursively in the form $\Delta u^n = (1-a\Delta t) \Delta u^{n-1} - \Delta t^2 \nabla E^n$.

3.3.1 The first order scheme as a sub-case of the second order scheme

For any choice of damping α_1 and time step Δt_1 parameters used in the first order scheme (denoted by subscript 1), we may obtain equivalent update iterations by substituting the following change of parameters into the second order scheme (denoted by subscript 2).

$$(30) \quad \Delta t_2 = \frac{\Delta t_1}{\sqrt{1 + \frac{a_1 \Delta t_1}{2}}} \quad \text{and} \quad a_2 = \frac{a_1}{\sqrt{1 + \frac{a_1 \Delta t_1}{2}}}$$

This is easily shown by algebraic simplification of the second order update (and stability condition) after applying the change of parameters. The simplified result will yield the first order scheme (and stability condition) in the original damping and time step parameters. In short, the first order scheme is always equivalent to the second order scheme with a reduced time step and damping via the contraction factor $\frac{1}{\sqrt{1 + \frac{a_1 \Delta t_1}{2}}} < 1$.

A particular special case of this equivalency arises in considering the maximal stable time step for both schemes. For a fixed choice of damping a , the first order scheme appears to allow a more generous upper bound than the second order scheme. However, there is no effective difference when substituting (30) into the second order scheme. Although the upper bound on the time step is smaller, the contracted time step is also smaller, such that the maximum stable time step in the first order scheme rescales exactly to the maximum stable time step in the second order scheme. Thus, so long as the damping is also contracted according to (30), the first order scheme implemented with its maximum stable time step is equivalent to the second order scheme implemented with its maximum stable time step.

We may also consider the backwards version of the change of parameters (30) in order to map the second order scheme into the first order scheme. In this case, using parameters a_2 and Δt_2 in the second order scheme is equivalent to applying the following change of parameters to the first order scheme.

$$(31) \quad \Delta t_1 = \frac{\Delta t_2}{\sqrt{1 - \frac{a_2 \Delta t_2}{2}}} \quad \text{and} \quad a_1 = \frac{a_2}{\sqrt{1 - \frac{a_2 \Delta t_2}{2}}}$$

However, this backwards mapping only applies when the second order parameters satisfy $a_2 \Delta t_2 < 2$. When this condition is satisfied, we can show by direct substitution and algebraic simplification, that the second order scheme (and stability condition) is equivalent to the first order scheme (and stability condition) with an amplified time step and damping coefficient via the amplification factor $\frac{1}{\sqrt{1 - \frac{a_2 \Delta t_2}{2}}} > 1$. Assuming the same condition is satisfied, the second order scheme implemented with its maximum stable time step is equivalent to the first order scheme implemented with its maximum stable time step after boosting the damping parameter according to (31).

3.3.2 Critical damping in the second order scheme (gradient descent)

Unlike the forward mapping of the first order into the second order discrete scheme, which is always possible for any choice of first order discrete parameters a_1 and Δt_1 , the backwards

mapping is not possible for certain choices of the second order discrete parameters, namely for $a_2\Delta t_2 \geq 2$ where the backwards amplification factor $\frac{1}{\sqrt{1-\frac{a_2\Delta t_2}{2}}}$ is undefined. While Δt_2 is upper-bounded by the second order scheme's stability constraint, there is no such upper-bound imposed on α_2 since the stability constraint is independent of α_2 . As such for any stable, nonzero, second-order discrete time step Δt_2 , we may always choose the second order discrete damping coefficient a_2 high enough to enter into this parameter regime where $a_2\Delta t_2 \geq 2$. In this case the second order scheme will exhibit behavior that is no longer reproducible by the first order scheme.

It is interesting to consider what happens at the transition point when $a_2\Delta t_2 = 2$. It is immediately seen, by plugging this into (29), that the second order scheme becomes identical to the discrete gradient descent scheme (27) with an effective gradient descent time step of $\Delta t = \frac{1}{2}\Delta t_2^2$ at this transition point (and if the second order accelerated time step Δt_2 was chosen to be the maximum stable step size of $2/\sqrt{z_{\max}}$, the effective gradient descent time step Δt will also be the maximum stable gradient descent step size of $2/z_{\max}$). If we fix the second order step size Δt_2 and approach the transition point $a_2 = 2/\Delta t_2$ from below, where an equivalent first order damping coefficient a_1 can be obtained via (31), then we see that the damping in the matching first order scheme becomes infinite as the damping in the second order scheme approaches this critical value. This constitutes a discrete analog of the continuum property that the continuous gradient descent PDE (17) arises as the infinite frictional limit of the continuous accelerated descent PDE (16).

If we want a damping value α_2 in the second order scheme that will always keep us below this transition point for all choices of stable time step, then we must satisfy the inequality $a_2\Delta t_2 < 2$ for the maximum stable step size of $2/\sqrt{z_{\max}}$. This leads to the following upper bound for the second order damping coefficient.

$$a_2 < \sqrt{z_{\max}}$$

Namely, the square of damping factor should be strictly less than the gradient amplifier.

3.3.3 Over-damping in the second order scheme (gradient descent with resistance)

Noting that gradient descent arises in both schemes (although only in the limiting sense for the first order scheme) at the transition point when $a_2\Delta t_2 = 2$, and that both schemes offer equivalent discretizations of accelerated descent according to the rescalings (30) and (31) below this transition point, it is now interesting to consider what happens above this transition point in the second order scheme. If we choose $a_2 > \sqrt{z_{\max}}$ then there will be stable time step choices for Δt_2 that will bring us beyond this transition.

In the case $a_2\Delta t_2 > 2$, the second order update, in its recursive form (29) becomes a weighted combination of a step in the negative gradient direction as well as a *backward* step in the previous update direction. As such, the combined step can be interpreted as *partially undoing* the previous step, thereby slowing down the descent process. If we take the limiting case as the second order damping coefficient a_2 becomes infinite (keeping the same fixed

time step Δt_2), the stability of the scheme will not be affected, but the new update will fully subtract the previous update, thereby returning to the previous state before applying the new gradient step. Furthermore, after subtracting the previous update the amount of movement along the new gradient step will be zero for infinite a_2 . This can be seen by noting that the weight on the previous update in (29) approaches -1 from above and that the weight on the gradient approaches 0 from below as $a_2 \rightarrow \infty$. Therefore, in the limit, even if we initialize the recursion (29) with a non-zero starting update Δu^0 (the discrete analog of an initial velocity), the effect will still be to remain motionless at the initial condition u^0 .

This leads to the interpretation of the over-damped case as a *resisted* version of gradient descent for any finite $\alpha_2 > 2/\Delta t_2$, since we start with a gradient step in the first update, then partially undo it before taking a new gradient step in the second update, which is then partially undone before taking a new gradient step in the third update, and so on. Since the fraction of each gradient step which gets subtracted in the subsequent step remains fixed, rather than accumulating, we do not refer to this as deceleration but rather as *resistance*, which impedes the normal progress of gradient descent by a constant factor. As a_2 increases, resistance increases, further slowing the progress of gradient descent, while completely halting it in the limit as $a_2 \rightarrow \infty$.

3.4 Semi-Implicit Schemes

We may use semi-implicit Euler style discretizations of (16) to obtain systems which more closely resemble the classic two-part Nesterov recursion. We may do this with any of the fully explicit schemes (21), (23), or (25) by replacing the explicit discretization ∇E^n of the gradient with a “predicted estimate” $\widehat{\nabla E}^{n+1}$ of its implicit discretization ∇E^{n+1} . This estimate is obtained by applying the same discretization of ∇E used in approximating $\nabla E^n \approx \nabla E(u^n)$ to a partial update v^n for the “look ahead” approximation $\widehat{\nabla E}^{n+1} \approx \nabla E(v^n)$. The partial update v^n is obtained beforehand via the fully explicit update without the gradient term (i.e. by treating ∇E^n as if it were zero). Using this strategy with the second order in time scheme (21) yields the following two-step update, where the first and second steps, in isolation, both have a fully explicit structure.

$$(32) \quad v^n = u^n + \frac{2 - a\Delta t}{2 + a\Delta t} \Delta u^{n-1} \quad \text{then} \quad u^{n+1} = v^n - \frac{2\Delta t^2}{2 + a\Delta t} \underbrace{\nabla E(v^n)}_{\approx \widehat{\nabla E}^{n+1}}$$

Von Neumann analysis can be employed to analyze the stability of this scheme according to the following update relationships between the DFT sequences U^n , V^n , and U^{n+1} (transforms of u^n , v^n , and u^{n+1} respectively) where $z(w)$ represents the gradient amplifier (19) associated

with the linearization of ∇E^n (and therefore also with the linearization of $\widehat{\nabla E}^{n+1}$).

$$\begin{aligned} V^n &= U^n + \frac{2 - a\Delta t}{2 + a\Delta t} (U^n - U^{n-1}) = \frac{4}{2 + a\Delta t} U^n - \frac{2 - a\Delta t}{2 + a\Delta t} U^{n-1} \\ U^{n+1} &= V^n - \frac{2\Delta t^2}{2 + a\Delta t} z(\omega) V^n = \left(1 - \frac{2\Delta t^2}{2 + a\Delta t} z(\omega)\right) V^n \end{aligned}$$

If we substitute the first expression into the second, followed by substitutions $U^{n\pm m} = \xi^{\pm m} U^n$, then we obtain the quadratic equation

$$\underbrace{(2 + a\Delta t)^2}_{A} \xi^2 - 4 \underbrace{(2 + a\Delta t - 2\Delta t^2 z(\omega))}_{-B} \xi + \underbrace{(2 - a\Delta t)(2 + a\Delta t - 2\Delta t^2 z(\omega))}_{C} = 0$$

for the overall combined update amplification factor $\xi(\omega)$. We may use the Root Amplitude Lemma to check the stability criterion $|\xi(\omega)| \leq 1$.

First stability condition: $A \geq C$ The first condition from the lemma (for positive A) can be expressed in quadratic form as $az\Delta t^2 - (a^2 + 2z)\Delta t - 2a \leq 0$ which will be satisfied between its positive and negative roots. Restricting our interest to only positive values of Δt therefore yields the constraint

$$\Delta t \leq \underbrace{\frac{a^2 + 2z + \sqrt{(a^2 + 2z)^2 + 8a^2 z}}{2az}}_{g(a,z)>0} \quad \text{where} \quad \frac{\partial g}{\partial a} = \underbrace{(a^2 - 2z)}_{\text{toggles}} \left(\underbrace{\frac{a^2 + 2z + \sqrt{(a^2 + 2z)^2 + 8a^2 z}}{2a^2 z \sqrt{(a^2 + 2z)^2 + 8a^2 z}}}_{\text{always positive}} \right)$$

To satisfy this independently of a , we examine the partial derivative of the upper bound $g(a, z)$ with respect to a see that it starts out negative for $a^2 < 2z$ then turns positive for $a^2 > 2z$. The minimum upper bound is therefore attained when $z(\omega) = z_{\max}$ and $a^2 = 2z_{\max}$ yielding

$$\Delta t \leq \frac{2 + \sqrt{2}}{\sqrt{z_{\max}}}$$

While this upper bound is more generous than (22) for the fully explicit scheme, it only satisfies the first of the two stability conditions in the Bounded Root Lemma. We now proceed to the second condition which will be more restrictive.

Second stability condition: $A + C \geq |B|$ The second condition from the lemma (for positive A) can be expressed as

$$2 + a\Delta t - \Delta t^2 z(\omega) + \frac{1}{2} a\Delta t^3 z(\omega) \geq |2 + a\Delta t - 2\Delta t^2 z(\omega)|$$

For small enough time steps, $2 + a\Delta t - 2\Delta t^2 z$ is positive, the absolute value signs can be removed, and the inequality holds. For larger time steps $2 + a\Delta t - 2\Delta t^2 z$ becomes and the inequality can be rearranged into the following cubic form

$$az(\omega)\Delta t^3 - 6z(\omega)\Delta t^2 + 4a\Delta t + 8 \geq 0$$

Minimizing on the left with the case $a = 0$ and $z(\omega) = z_{\max}$ yields a stricter, and therefore sufficient, stand-alone stability condition

$$(33) \quad \Delta t \leq \frac{2}{\sqrt{3z_{\max}}}$$

Note that this upper bound is smaller, by a factor of $\sqrt{3}$, than the maximum stable time step (22) for the corresponding fully explicit scheme (21) or for its recursive equivalent (29).

4 Regularized Inversion via Accelerated PDEs

Here we consider a very general class of variational regularized inversion problems in the accelerated PDE framework. In particular, we assume energy functions with the form

$$E(u) = \int_{\Omega} \underbrace{f(|\mathcal{K}u - g|)}_{\text{fidelity}} + \underbrace{r(\|\nabla u\|)}_{\text{regularity}} dx, \quad \text{with } \dot{f}, \dot{r}, \ddot{r} > 0$$

where f is a monotonically increasing penalty on the residual error between data measurements g and a forward in the form of linear operator \mathcal{K} applied to the reconstructed signal u , while r is a monotonically increasing penalty on the gradient of the reconstruction.

4.1 General Case (nonlinear wave equation)

The continuum gradient of E has the form

$$\begin{aligned} \nabla E(u) &= \frac{\dot{f}(|\mathcal{K}u - g|)}{|\mathcal{K}u - g|} \mathcal{K}^* (\mathcal{K}u - g) - \dot{r}(\|\nabla u\|) \nabla \cdot \left(\frac{\nabla u}{\|\nabla u\|} \right) - \ddot{r}(\|\nabla u\|) \frac{\nabla u^T \nabla^2 u \nabla u}{\|\nabla u\|^2} \\ &= \underbrace{\frac{\dot{f}(|\mathcal{K}u - g|)}{|\mathcal{K}u - g|} \mathcal{K}^* (\mathcal{K}u - g)}_{\lambda(u,x) > 0} - \underbrace{\frac{\dot{r}(\|\nabla u\|)}{\|\nabla u\|}}_{c(\nabla u) > 0} (\nabla \cdot \nabla u - u_{\eta\eta}) - \underbrace{\ddot{r}(\|\nabla u\|)}_{d(\nabla u) > 0} u_{\eta\eta} \end{aligned}$$

where \mathcal{K}^* denotes the adjoint of the forward operator \mathcal{K} , and where $\eta \doteq \frac{\nabla u}{\|\nabla u\|}$ denotes the unit vector along the gradient direction of u . This gives rise to the following class of accelerated flows which take the form of a nonlinear wave equation.

$$(34) \quad u_{tt} - c(\nabla u) (\nabla \cdot \nabla u - u_{\eta\eta}) - d(\nabla u) u_{\eta\eta} + au_t = \lambda(u, x) \mathcal{K}^* (g - \mathcal{K}u)$$

If, purely for the sake of understanding stability, we model the short time behavior of any of the presented discrete update schemes in the neighborhood of a particular spatial point x , by treating λ , c , and d as locally constant, and by representing the forward model linear operator \mathcal{K} as a real convolution kernel K with adjoint K^T , then ∇E can be approximated near x by the following linear expression

$$(35) \quad \nabla E \approx \lambda_{[x]} K_{[x]}^T * K_{[x]} * (u^n - g) - c_{[x]} (\nabla \cdot \nabla u^n - u_{\eta\eta}) + d_{[x]} u_{\eta\eta}$$

where the subscript $[x]$ denotes the local point of spatially constant approximation (rather than a function argument). Assuming a uniform Cartesian grid oriented such that its first basis vector $\vec{e}_1 = (1, 0, 0, \dots)$ aligns with ∇u at our local point x , and that our spatial derivative discretizations become equivalent to central difference (second derivative) approximations with space step Δx in each direction, then we obtain the following local approximation of the gradient amplifier of (35)

$$(36) \quad \begin{aligned} z(x, \omega_1, \omega_2, \dots, \omega_N) \approx & \lambda_{[x]} \text{DFT}(K_{[x]}^T) \text{DFT}(K_{[x]}) \\ & + \frac{2}{\Delta x^2} \left(d_{[x]} (1 - \cos \omega_1 \Delta x) + c_{[x]} \sum_{k=2}^N (1 - \cos \omega_k \Delta x) \right) \end{aligned}$$

Noting that the Fourier transform of the adjoint K^T of a real convolution kernel is always the complex conjugate of the Fourier transform of the kernel K itself, we see that the gradient amplifier is real and positive and we can write the following upper bound as a function frequency ω

$$\max_{\omega} z \leq \lambda_{[x]} \max_{\omega} |\text{DFT}(K_{[x]})|^2 + 4 \frac{c_{[x]} (N - 1) + d_{[x]}}{\Delta x^2}$$

with equality in cases where the complex amplitude of $\text{DFT}(K)$ is maximal at $\omega = (\pi, \dots, \pi)$. However, since this upper bound depends on the local point of approximation x , we need to maximize over x as well in order to exploit the CFL formulas presented earlier in terms of z_{\max} . Doing so yields the following upper bound for the local gradient amplifier.

$$(37) \quad \begin{aligned} z_{\max} \leq \max_{x, \omega} (|\text{DFT}(K)|^2) \lambda_{\max} + 4 \frac{(N - 1)c_{\max} + d_{\max}}{\Delta x^2} \\ \text{where } \lambda_{\max} \doteq \max_x \lambda, \quad c_{\max} \doteq \max_x c, \quad d_{\max} \doteq \max_x d \end{aligned}$$

If we now plug (37) into the time step restriction (22) for the fully explicit second order accelerated scheme (21), we obtain the following sufficient condition for stability

$$(38) \quad \Delta t \leq \frac{2\Delta x}{\sqrt{\max (|\text{DFT}(K)|^2) \lambda_{\max} \Delta x^2 + 4(N - 1)c_{\max} + 4d_{\max}}}$$

The corresponding condition for gradient descent is obtained by squaring Δx in the numerator and removing the radical (squaring) the denominator. As such we note three favorable step size trends for PDE acceleration compared to PDE gradient descent. Most notably,

when the regularizing coefficients c_{\max} and d_{\max} dominate, stable time step sizes are now directly proportional to spatial step sizes rather than to their squares, making the upper bound linear rather than quadratic in Δx . We see similar gains as well when the kernel K exhibits large amplification at one or more frequencies. In such cases, stable step sizes are inversely proportional to the maximum kernel amplification rather than to its square.

4.2 Quadratic regularization (linear wave equation)

The easiest special case to consider would be that of quadratic fidelity and regularity penalties without any forward model (more precisely, with \mathcal{K} as the identity operator).

$$E(u) = \int_{\Omega} \frac{\lambda}{2} (u - g)^2 + \frac{c}{2} \|\nabla u\|^2 dx$$

In this case the gradient is linear and the local approximation (35) becomes exact with $\lambda(x) = \lambda$, $c(x) = d(x) = c$.

$$\nabla E = \lambda(u - g) - c \nabla \cdot \nabla u$$

The accelerated descent PDE therefore takes the form of a damped inhomogeneous linear wave equation.

$$(39) \quad u_{tt} - c \nabla \cdot \nabla u + au_t = \lambda(g - u)$$

In this case the gradient amplifier $z(\omega)$ (19) is easy to compute. If central differences on a uniform N -dimensional Cartesian grid with space step Δx in each direction are used to approximate the spatial derivatives of the Laplacian $\nabla \cdot \nabla$, then

$$z(\omega) = \lambda + \frac{2c}{\Delta x^2} \sum_{k=1}^N (1 - \cos \omega_k \Delta x), \quad \omega = (\omega_1, \dots, \omega_N)$$

which makes the local approximation (36) exact as well. Its upper bound

$$(40) \quad z_{\max} = \lambda + \frac{4Nc}{\Delta x^2}$$

is attained at $\omega = (\pi, \dots, \pi)$, thereby making the general condition (38) necessary as well as sufficient for stability. Plugging all this into (27), (28), and (29) yields the following fully explicit updates (and CFL conditions), with multi-index $\alpha = (\alpha_1, \alpha_2, \dots, \alpha_N)$ to indicate each grid location, and where the additive multi-index $e_k = (\delta_{1k}, \delta_{2k}, \dots, \delta_{Nk})$ is used to

denote displacements to adjacent grid neighbors (δ_{jk} being the standard Kronecker delta).

(41)

$$\text{gradient descent} \begin{cases} \Delta u_\alpha^n = -\Delta t \left(\lambda(u_\alpha^n - g_\alpha) - c \sum_{k=1}^N \frac{u_{\alpha+e_k}^n - 2u_\alpha^n + u_{\alpha-e_k}^n}{\Delta x^2} \right) \\ \Delta t \leq \frac{2\Delta x^2}{4Nc + \lambda\Delta x^2} \end{cases}$$

(42)

$$\text{1-order accelerated} \begin{cases} \Delta u_\alpha^n = \frac{1}{1+a\Delta t} \Delta u_\alpha^{n-1} - \frac{\Delta t^2}{1+a\Delta t} \left(\lambda(u_\alpha^n - g_\alpha) - c \sum_{k=1}^N \frac{u_{\alpha+e_k}^n - 2u_\alpha^n + u_{\alpha-e_k}^n}{\Delta x^2} \right) \\ \Delta t \leq \Delta x \sqrt{\frac{4}{4Nc + \lambda\Delta x^2} + \left(\frac{a\Delta x}{4Nc + \lambda\Delta x^2} \right)^2} + \frac{a\Delta x^2}{4Nc + \lambda\Delta x^2} \end{cases}$$

(43)

$$\text{2-order accelerated} \begin{cases} \Delta u_\alpha^n = \frac{2-a\Delta t}{2+a\Delta t} \Delta u_\alpha^{n-1} - \frac{2\Delta t^2}{2+a\Delta t} \left(\lambda(u_\alpha^n - g_\alpha) - c \sum_{k=1}^N \frac{u_{\alpha+e_k}^n - 2u_\alpha^n + u_{\alpha-e_k}^n}{\Delta x^2} \right) \\ \Delta t \leq \frac{2\Delta x}{\sqrt{4Nc + \lambda\Delta x^2}} \end{cases}$$

(44)

$$\text{semi-implicit} \begin{cases} v_\alpha^n = u_\alpha^n + \frac{2-a\Delta t}{2+a\Delta t} \Delta u^{n-1} \\ u_\alpha^{n+1} = v_\alpha^n - \frac{2\Delta t^2}{2+a\Delta t} \left(\lambda(v_\alpha^n - g_\alpha) - c \sum_{k=1}^N \frac{v_{\alpha+e_k}^n - 2v_\alpha^n + v_{\alpha-e_k}^n}{\Delta x^2} \right) \\ \Delta t \leq \frac{2\Delta x}{\sqrt{3(4Nc + \lambda\Delta x^2)}} \quad (\text{sufficient but not necessary when } a > 0) \end{cases}$$

4.3 Implicit handling of the fidelity term

The portion of the continuum gradient which arises from the fidelity term is $\lambda(u - g)$, which we have discretized explicitly in the above schemes as $\lambda(u_\alpha^n - g_\alpha)$. Since this term, unlike the Laplacian discretization, does not depend upon neighboring grid locations, we could evaluate it implicitly at the updated value of u by plugging $\lambda(u_\alpha^{n+1} - g_\alpha)$ into any of these schemes and yet still rearrange the resulting expressions to obtain explicit updates for u_α^{n+1} . Algebraic manipulation of these resulting implicitly handled fidelity schemes would yield the following equivalent schemes, restructured to reveal their similarity to the schemes (41), (42), (43),

and (44) shown above.

(45)

$$\text{gradient descent: } \Delta u_\alpha^n = -\frac{\Delta t}{1 + \lambda \Delta t} \left(\lambda(u_\alpha^n - g_\alpha) - c \sum_{k=1}^N \frac{u_{\alpha+e_k}^n - 2u_\alpha^n + u_{\alpha-e_k}^n}{\Delta x^2} \right)$$

(46)

$$\text{1-order accelerated: } \Delta u_\alpha^n = \frac{\Delta u_\alpha^{n-1} - \Delta t^2 \left(\lambda(u_\alpha^n - g_\alpha) - c \sum_{k=1}^N \frac{u_{\alpha+e_k}^n - 2u_\alpha^n + u_{\alpha-e_k}^n}{\Delta x^2} \right)}{1 + (a + \lambda \Delta t) \Delta t}$$

(47)

$$\text{2-order accelerated: } u_\alpha^n = \frac{(2 - a \Delta t) \Delta u_\alpha^{n-1} - 2 \Delta t^2 \left(\lambda(u_\alpha^n - g_\alpha) - c \sum_{k=1}^N \frac{u_{\alpha+e_k}^n - 2u_\alpha^n + u_{\alpha-e_k}^n}{\Delta x^2} \right)}{2 + a \Delta t + 2 \lambda \Delta t^2}$$

$$(48) \quad \text{semi-implicit: } \begin{cases} v_\alpha^n = u_\alpha^n + \frac{2-a\Delta t}{2+a\Delta t} \Delta u^{n-1} \\ u_\alpha^{n+1} = v_\alpha^n - \frac{2\Delta t^2}{2+a\Delta t+2\lambda\Delta t^2} \left(\lambda(v_\alpha^n - g_\alpha) - c \sum_{k=1}^N \frac{v_{\alpha+e_k}^n - 2v_\alpha^n + v_{\alpha-e_k}^n}{\Delta x^2} \right) \end{cases}$$

Written in this form it is easy to show by comparison that these schemes become equivalent to their explicit-fidelity counterparts by a change of time step, damping parameter, or both. In the case of gradient descent, the implicit-fidelity scheme (45) is identical to explicit-fidelity scheme (41) with a smaller time step, using $\Delta t \rightarrow \frac{\Delta t}{1+\lambda\Delta t}$. The first order implicit-fidelity accelerated scheme (46) is equivalent to its explicit-fidelity counterpart (42) with a larger damping coefficient, using $a \rightarrow a + \lambda\Delta t$. The second order implicit-fidelity accelerated scheme (47) is equivalent to the explicit-fidelity scheme (43) with both a smaller time step and an adjusted damping coefficient (may be either larger or smaller depending on λ), using $\Delta t \rightarrow \frac{\Delta t}{\sqrt{1+\frac{\lambda}{2}\Delta t^2}}$ and $a \rightarrow \frac{a+\lambda\Delta t}{\sqrt{1+\frac{\lambda}{2}\Delta t^2}}$. Finally the implicit-fidelity adaptation (48) of the semi-implicit scheme (44), obtained by replacing $\lambda(u_\alpha^{n+1} - g)$ with $\lambda(v_\alpha^n - g)$, is equivalent to the original semi-implicit scheme (44) with both a smaller time step and a larger damping coefficient, using $\Delta t \rightarrow \frac{\Delta t}{\sqrt{1+\frac{2\lambda\Delta t^2}{2+a\Delta t}}}$ and $a \rightarrow a\sqrt{1+\frac{2\lambda\Delta t^2}{2+a\Delta t}}$.

The CFL conditions for these implicit-fidelity schemes can therefore be obtained by applying these substitutions backwards to the matching explicit (or semi-implicit) CFL conditions. While this often yields a larger maximum stable time step, the apparent gain is deceptive since there is will be no numerical difference to the corresponding explicit (or semi-implicit) update with a smaller time step. As such, there is neither a computational nor a numerical advantage to handling the fidelity term implicitly. While we have illustrated this here for the special case of quadratic regularization, the parameter remappings showing equivalency between the explicit and partially implicit schemes depend only upon the damping and fidelity parameters. It is easy to see that the exact same analysis applies even in the nonlinear case of non-quadratic regularization, making this equivalency (and therefore the lack of benefit in implicitly handling the fidelity) more general.

Further generalization of this analysis is also possible in the accelerated cases for non-quadratic fidelity penalization as well as for nontrivial forward models \mathcal{K} . However, in such

cases, equivalency would require substitution of a constant damping parameter α in the partially implicit scheme with a spatially varying damping in the equivalent explicit scheme. For example, in the case of a quadratic fidelity penalty paired with a convolution kernel K in the first order accelerated implicit-fidelity scheme (46), a constant damping parameter a would have to be replaced by the spatially varying $a\mathcal{I} + \lambda\Delta t K^T K$ in order to use the explicit-fidelity scheme (42) to obtain equivalent updates. This would require inversion of the matrix $(1 + a\Delta t)\mathcal{I} + \lambda\Delta t^2 K^T K$, as division by a scalar would no longer occur in the explicit update (42). However since this inverse does not depend on u , it inverse could be computed/approximated just once and then reused in every update step (in cases where the damping does not change with time).

4.4 Beltrami regularization (quasi-linear wave equation)

Another special case to consider is Beltrami regularization. We'll consider the case of a quadratic penalty and an attenuating, mean-preserving convolution kernel K

$$(49) \quad E(u) = \int_{\Omega} \frac{\lambda}{2} (K * u - g)^2 + \underbrace{\frac{1}{\beta} \sqrt{1 + \|\beta \nabla u\|^2}}_{\sqrt{\epsilon^2 + \|\nabla u\|^2}, \epsilon = \frac{1}{\beta}} dx$$

In this case the variational gradient is non-linear and (35) decomposes as follows.

$$\begin{aligned} \nabla E &= \lambda K^T * K * (u - g) - \nabla \cdot \left(\underbrace{\frac{\beta \nabla u}{\sqrt{1 + \|\beta \nabla u\|^2}}}_{\frac{\nabla u}{\sqrt{\epsilon^2 + \|\nabla u\|^2}}, \epsilon = \frac{1}{\beta}} \right) \\ &= \lambda K^T * K * (u - g) - \underbrace{\frac{\beta}{\sqrt{1 + \|\beta \nabla u\|^2}}}_{c} (\nabla \cdot \nabla u - u_{\eta\eta}) - \underbrace{\frac{\beta}{(\sqrt{1 + \|\beta \nabla u\|^2})^3}}_d u_{\eta\eta} \end{aligned}$$

while the accelerated PDE (technically an integral partial differential equation with the convolution) takes the quasilinear form.

$$(50) \quad u_{tt} - \nabla \cdot \left(\frac{\beta \nabla u}{\sqrt{1 + \|\beta \nabla u\|^2}} \right) + au_t = \lambda K^T * K * (g - u)$$

Note that both coefficients c and d are bounded by β (an upper bound which is actually reached in both cases at any point and time where $\nabla u(x, t) = 0$), and that $\max |\text{DFT}(K)| = 1$ by our assumption that K attenuates while preserving the mean. Plugging this into (37) yields

$$(51) \quad z_{\max} \leq \lambda + \frac{4N\beta}{\Delta x^2}$$

if we assume a consistent discretization of $\nabla \cdot \left(\frac{\beta \nabla u}{\sqrt{1 + \|\beta \nabla u\|^2}} \right)$ which converges, as $\nabla u \rightarrow 0$, to the central difference approximation of the β -scaled Laplacian $\beta \nabla \cdot \nabla u \approx \beta \sum_{k=1}^N \frac{u_{\alpha+e_k}^n - 2u_{\alpha}^n + u_{\alpha-e_k}^n}{\Delta x^2}$ with spatial step size Δx in each direction (see Section (4.2) for the multi-index subscript notation α and e_k). If we let $D_{\beta, \Delta x}^2 u^n$ denote the discretization of $\nabla \cdot \left(\frac{\beta \nabla u}{\sqrt{1 + \|\beta \nabla u\|^2}} \right)$ then we obtain the following schemes

$$(52) \quad \text{gradient descent} \begin{cases} \Delta u^n = -\Delta t (\lambda K^T * K * (u^n - g) - D_{\beta, \Delta x}^2 u^n) \\ \Delta t \leq \Delta x^2 \left(\frac{2}{4N\beta + \lambda \Delta x^2} \right) \end{cases}$$

$$(53) \quad \text{1-order accelerated} \begin{cases} \Delta u^n = \frac{1}{1+a\Delta t} \Delta u^{n-1} - \frac{\Delta t^2}{1+a\Delta t} (\lambda K^T * K * (u^n - g) - D_{\beta, \Delta x}^2 u^n) \\ \Delta t \leq \Delta x \left(\sqrt{\frac{4}{4N\beta + \lambda \Delta x^2} + \left(\frac{a\Delta x}{4N\beta + \lambda \Delta x^2} \right)^2} + \frac{a\Delta x}{4N\beta + \lambda \Delta x^2} \right) \end{cases}$$

$$(54) \quad \text{2-order accelerated} \begin{cases} \Delta u^n = \frac{2-a\Delta t}{2+a\Delta t} \Delta u^{n-1} - \frac{2\Delta t^2}{2+a\Delta t} (\lambda K^T * K * (u^n - g) - D_{\beta, \Delta x}^2 u^n) \\ \Delta t \leq \Delta x \left(\frac{2}{\sqrt{3(4N\beta + \lambda \Delta x^2)}} \right) \end{cases}$$

$$(55) \quad \text{semi-implicit} \begin{cases} v^n = u^n + \frac{2-a\Delta t}{2+a\Delta t} \Delta u^{n-1} \\ u^{n+1} = v^n - \frac{2\Delta t^2}{2+a\Delta t} (\lambda K^T * K * (v^n - g) - D_{\beta, \Delta x}^2 v^n) \\ \Delta t \leq \Delta x \left(\frac{2}{\sqrt{3(4N\beta + \lambda \Delta x^2)}} \right) \end{cases}$$

4.5 Total Variation Regularization

If we consider the limit as $\beta \rightarrow \infty$, the Beltrami regularization penalty converges to the total variation penalty.

$$(56) \quad E(u) = \int_{\Omega} \frac{\lambda}{2} (K * u - g)^2 + \|\nabla u\| dx$$

with a non-linear variational gradient (35) that decomposes as follows.

$$\nabla E = \lambda K^T * K * (u - g) - \nabla \cdot \left(\frac{\nabla u}{\|\nabla u\|} \right) = \lambda K^T * K * (u - g) - \underbrace{\frac{1}{\|\nabla u\|}}_c (\nabla \cdot \nabla u - u_{\eta\eta})$$

The accelerated PDE now takes the form of the following nonlinear wave equation.

$$(57) \quad u_{tt} - \nabla \cdot \left(\frac{\nabla u}{\|\nabla u\|} \right) + au_t = \lambda K^T * K * (g - u)$$

In this case, the coefficient d vanishes, but the coefficient c no longer has a finite upper bound. Plugging this into (37) yields an infinite upper bound for the maximum gradient

amplifier if at any point and time $\nabla u(x, t) = 0$. Otherwise, by our earlier assumption on K (see Section 4.4) we obtain

$$(58) \quad \lambda \leq z_{\max} \leq \lambda + \frac{4(N-1)}{\Delta x^2 \min \|\nabla u\|}.$$

For the explicit second order accelerated scheme, this ensures the sufficient condition $\Delta t \leq \frac{2}{\sqrt{\lambda + \frac{4(N-1)}{\Delta x^2 \min \|\nabla u\|}}}$ for a stable step. If we fix Δt , we may rearrange this inequality to obtain an equivalent sufficient condition

$$\min \|\nabla u\| \geq \frac{N-1}{\Delta x^2} \frac{4\Delta t^2}{4 - \lambda\Delta t^2}$$

which takes the form of a lower bound on the spatial gradient.

Here an interesting nonlinear dynamic occurs to keep the implementation stable by preventing initiated instabilities from growing unbounded. If the spatial gradient falls below this lower bound and instabilities begins to propagate at one or more frequencies, they will eventually cause the spatial gradient to rise above the guaranteed stable lower bound at which point the instabilities will cease growing. In the absence of a kernel K , the fastest growing instability will occur at the highest digital frequency in each grid direction $\omega = (\pi, \dots, \pi)$ which corresponds to oscillations between immediately adjacent grid-points, this in turn will most rapidly increase the discrete difference approximations of $\|\nabla u\|$. In the presence of a strongly smoothing kernel, the fastest growing instability may occur at lower digital frequencies, thereby causing a low-grade ringing effect, with several grid-points per period, until the amplitude of the oscillation is large enough to drive adjacent pixel differences back over the lower bound for $\|\nabla u\|$.

A similar phenomenon occurs with both the first-order and semi-implicit schemes (and even with gradient descent), making all these schemes stable independently of the regularizer coefficient c . As such, purely for stability considerations alone, the necessary step size constraint will be connected to the lower bound λ of the gradient amplifier z_{\max} rather than its upper bound in (58). This yields the following necessary conditions for stability.

$$(59) \quad \text{gradient descent: } \Delta t \leq \frac{2}{\lambda}$$

$$(60) \quad \text{1-order accelerated: } \Delta t \leq \sqrt{\frac{4}{\lambda} + \left(\frac{a}{\lambda}\right)^2} + \frac{a}{\lambda}$$

$$(61) \quad \text{2-order accelerated: } \Delta t \leq \frac{2}{\sqrt{\lambda}}$$

$$(62) \quad \text{semi-implicit: } \Delta t \leq \frac{2}{\sqrt{3\lambda}}$$

However, the schemes may only converge under these constraints in an oscillatory sense with a fluctuating level of “background noise” whose amplitude will depend upon the value of Δt .

We may exploit the behavior of this non-linear stabilizing effect to obtain a more useful time step constraint by plugging in a minimal acceptable value of $\|\nabla u\|$ for the final reconstruction into the stability condition for Δt . A natural way to approach this is by exploiting a quantization interval Q for the digital representation of u together with the following discrete approximation bounds for $\|\nabla u\|$.

$$\min_{\alpha} \|\nabla u\| = \min_{\alpha} \sqrt{\sum_{k=1}^N \left(\frac{u_{\alpha+e_k} - u_{\alpha}}{\Delta x} \right)^2} \geq \sqrt{N \min_{\alpha,k} \left(\frac{u_{\alpha+e_k} - u_{\alpha}}{\Delta x} \right)^2} = \frac{\sqrt{N}}{\Delta x} \min_{\alpha,k} |u_{\alpha+e_k} - u_{\alpha}|$$

If we now determine that instability related distortions confined to a single quantization interval Q between neighboring pixels are acceptable, we substitute

$$\min \|\nabla u\| \rightarrow \frac{\sqrt{N}}{\Delta x} Q$$

into the upper bound for (58) to obtain

$$(63) \quad z_{\max} \leq \lambda + \frac{4(N-1)}{Q\Delta x\sqrt{N}} < \lambda + \frac{4\sqrt{N}}{Q\Delta x}$$

within the desired stable regime for $\|\nabla u\|$. This in turn gives rise to the following schemes, where $D_{\Delta x}^2 u^n$ denotes the discretization of $\nabla \cdot \left(\frac{\nabla u}{\|\nabla u\|} \right)$

$$(64) \quad \text{gradient descent} \begin{cases} \Delta u^n = -\Delta t (\lambda K^T * K * (u^n - g) - D_{\Delta x}^2 u^n) \\ \Delta t \leq Q\Delta x \left(\frac{2}{4\sqrt{N} + \lambda Q\Delta x} \right) \end{cases}$$

$$(65) \quad \text{1-order accelerated} \begin{cases} \Delta u^n = \frac{1}{1+a\Delta t} \Delta u^{n-1} - \frac{\Delta t^2}{1+a\Delta t} (\lambda K^T * K * (u^n - g) - D_{\Delta x}^2 u^n) \\ \Delta t \leq \sqrt{Q\Delta x} \left(\sqrt{\frac{4}{4\sqrt{N} + \lambda Q\Delta x} + \left(\frac{a\sqrt{Q\Delta x}}{4\sqrt{N} + \lambda Q\Delta x} \right)^2} + \frac{a\sqrt{Q\Delta x}}{4\sqrt{N} + \lambda Q\Delta x} \right) \end{cases}$$

$$(66) \quad \text{2-order accelerated} \begin{cases} \Delta u^n = \frac{2-a\Delta t}{2+a\Delta t} \Delta u^{n-1} - \frac{2\Delta t^2}{2+a\Delta t} (\lambda K^T * K * (u^n - g) - D_{\Delta x}^2 u^n) \\ \Delta t \leq \sqrt{Q\Delta x} \left(\sqrt{\frac{4}{4\sqrt{N} + \lambda Q\Delta x}} \right) \end{cases}$$

$$(67) \quad \text{semi-implicit} \begin{cases} v^n = u^n + \frac{2-a\Delta t}{2+a\Delta t} \Delta u^{n-1} \\ u^{n+1} = v^n - \frac{2\Delta t^2}{2+a\Delta t} (\lambda K^T * K * (v^n - g) - D_{\Delta x}^2 v^n) \\ \Delta t \leq \sqrt{Q\Delta x} \left(\sqrt{\frac{4}{3(4\sqrt{N} + \lambda Q\Delta x)}} \right) \end{cases}$$

5 Experimental Examples

5.1 Beltrami Denoising

Our first application is to the problem of Beltrami regularization for image denoising and image inpainting [13, 18, 27], which corresponds to minimizing (49) in the absence of a kernel

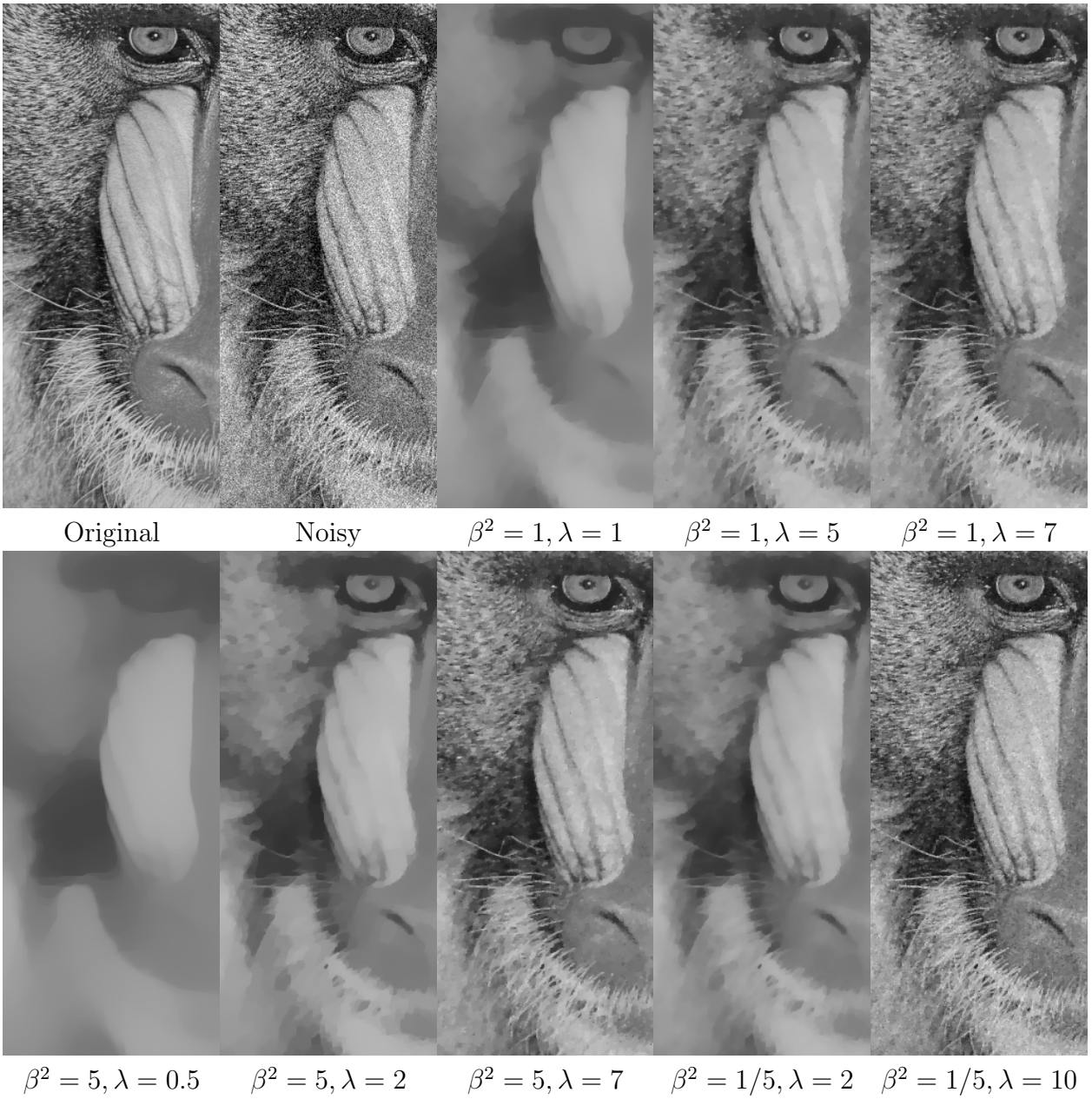


Figure 1: Results of Beltrami regularization applied to a noisy baboon image with varying values of λ and β . The units of λ are thousands.

	$\lambda = 1000$		$\lambda = 5000$		$\lambda = 7000$	
	Time	Iterations	Time	Iterations	Time	Iterations
$\beta^2 = 1/5$	0.55s	124	0.27s	60	0.23s	50
$\beta^2 = 1$	0.81s	183	0.38s	85	0.32s	71
$\beta^2 = 5$	1.20s	273	0.54s	122	0.45s	101

Table 1: PDE accelerated Beltrami regularization runtimes on the 512×512 baboon image.

K via the accelerated PDE (50). In this case g is the original noisy image, and the minimizer u is the denoised/inpainted image. For denoising we typically set the parameter λ to be a positive constant, and for inpainting we can set $\lambda = 0$ in the region $D \subset \Omega$ to be inpainted, and set λ to be large or ∞ in $\Omega \setminus D$. The Beltrami regularization term interpolates between the TV norm $\int |\nabla u|$ and the H^1 norm $\int |\nabla u|^2$ —near edges where ∇u is large, it behaves like the TV norm to preserve edges, and where ∇u is small it behaves like the H^1 norm in order to reduce staircasing. Recently, Zosso and Bustin [27] proposed an efficient primal dual projected gradient method for solving Beltrami regularized problems.

We use the first order explicit scheme (53) with forward differences for ∇u and backward differences for div . We set the damping coefficient to $a = 2\sqrt{\beta\pi^2 + \lambda}$, via the linear analysis (14) and run the algorithm at its maximum stable step Δt (53) until the absolute difference between the current and previous iterate falls below 10^{-4} . We note that the image is normalized so the pixel values fall in the interval $[0, 1]$.

Figure 1 shows the results of applying the PDE accelerated Beltrami regularization to a noisy baboon test image with varying values of λ and β with single-threaded C++ code on a 3.2 GHz Intel processor running Linux. The corresponding runtimes are given in Table 1 and are favorably competitive with the runtimes reported in [27], who proposed a primal dual projected gradient algorithm for Beltrami regularization. Notice the algorithm does slow down somewhat when λ is small and the denoising is heavily regularized, but the difference is far less pronounced compared to other explicit methods such as gradient descent.

5.2 Beltrami Inpainting

We also give an example of PDE acceleration for Beltrami regularized inpainting in Figure 2. We used $\beta = 1$ and $a = 5\pi$, and the inpainting took 687 iterations (11.48 seconds) starting from an initial guess given by nearest neighbor interpolation. This is a good deal slower than the denoising examples. It is possible to give a partial explanation for this. Recall that the optimal damping parameter, and convergence rate, depends on the size of the first eigenvalue of the linearized operator on the given domain, and the presence of a zeroth order term λu . In inpainting, there is no zeroth order term and the domain is highly irregular. Further, the inpainting domain is typically disconnected, so the eigenvalues on each connected component would be required, and this would lead to different choices of damping coefficient in each region. We plan to investigate this issue, and others, in future work.



(a) Original



(b) Corrupted



(c) Inpainting result ($\beta = 1$)



(d) Inpainting Enlarged

Figure 2: An example of inpainting using the PDE accelerated Beltrami regularization framework on the cameraman image.



Figure 3: Deblurring of an image using the explicit accelerated PDE scheme compared with the results of two other state of the art methods (final signal-to-noise ratios shown for each restoration).

5.3 Beltrami Deblurring

Finally, we give an example of PDE acceleration for Beltrami regularized deblurring. We used $\lambda = 10^7$, $\beta = 1$, and $a = 4$ and the deblurring was run using the second order explicit scheme (54) with its maximum stable time step starting with the original blurred image as the initial guess. After 2038 iterations it achieved its tenth-of-a-decibel rounded steady-state restored PSNR of 32.3dB. The original image was blurred with a Gaussian kernel of $\sigma = 3$ to create an blurry initial image with a signal-to-noise ratio of 25.6185dB. In Figure 3 we compare the accelerated PDE results, both visually as well as quantitatively according to the restored signal-to-noise ratio, with those obtained using primal dual and L1 ADMM algorithms for the same parameters $\lambda = 10^7$ and $\beta = 1$. ADMM reached its tenth-of-a-decibel rounded steady-state restored PSNR of 31.8dB after 2453 iterations, whereas Primal Dual reached its tenth-of-a-decibel rounded steady-state restored PSNR of 27.8dB after 63 iterations (significantly fewer iterations than both other algorithms, but also significantly lower restored PSNR).

5.4 TV Denoising

We now consider the problem of Total Variation (TV) restoration, which has a long history in image processing [17]. The TV denoising problem corresponds to minimizing (56) in the absence of a kernel K via the accelerated PDE (57). In this case state of the art approaches include primal dual methods [7] and the split Bregman method [9].

We again use the first order explicit scheme (65), while discretizing the spatial gradient and divergence separately (using forward differences for the gradient and backward differences for the divergence), and homogeneous Neumann boundary conditions. Numerically, we set $\nabla u / |\nabla u| = 0$ whenever $\nabla u = 0$, so no regularization is required, though we rarely encounter numerical gradients that are identically zero. This choice of discretization makes the discrete divergence the exact numerical adjoint of the discrete gradient.

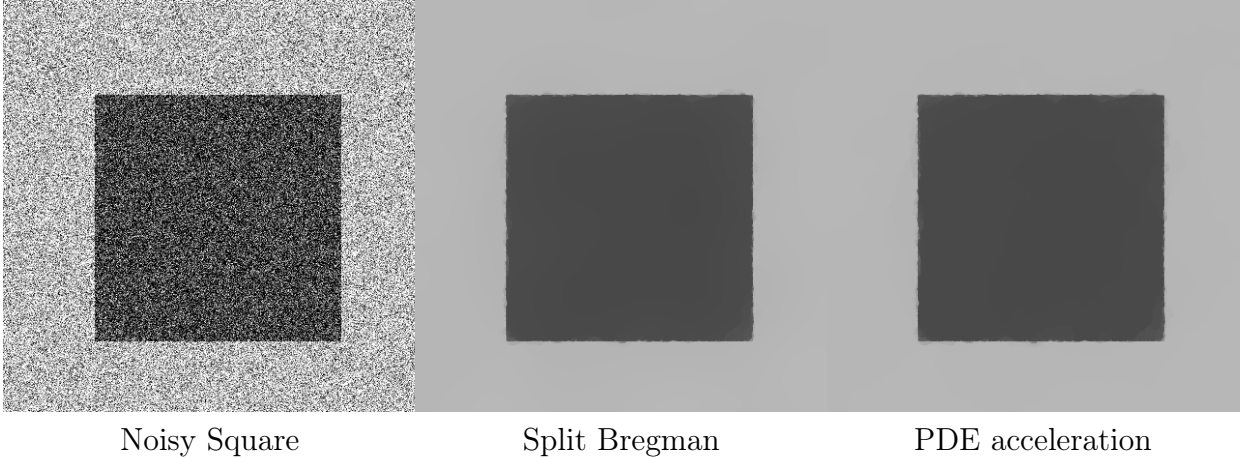


Figure 4: Denoising of a synthetic image with total variation restoration with $\lambda = 1000$ via (b) Split Bregman and (c) PDE acceleration. In PDE acceleration we used $\Delta t = \Delta x/2$ and $a = 6\sqrt{\lambda}$.

We first consider a noisy square image, with dark region $u = 0.25$ and light region $u = 0.75$ with additive Gaussian noise with standard deviation $\sigma = 0.3$. Figure 4 shows the noisy square and the total variation denoising with the Split Bregman algorithm and PDE acceleration. We compare PDE acceleration, Primal Dual, and Split Bregman on slices of the image at similar computation times in Figure 5. Notice the Primal Dual algorithm blurs the edges slightly at first, and they are restored only late in the flow (at $t = 4$ Primal dual has not yet converged). The PDE acceleration algorithm does a better job preserving edges (they are never blurred) compared to Primal Dual, and is slightly better than Split Bregman at preserving edges by time $t = 4$.

In the example above we took $\Delta t = \Delta x/2$ for simplicity. Corroborating our analysis in Section 4.5, this explicit numerical scheme (65) behaves stably in L^∞ in our experiments, meaning the solutions remain bounded in L^∞ for all time, even for larger time steps which still satisfy the necessary conditions (59), (60), (61) or (62). For such larger time steps, though, we find the flow does not fully converge, yet remains stable via the nonlinear effect discussed in Section 4.5, but instead tends to an oscillatory steady state. Figure 7 shows a snapshot of the steady state for various values of the time step Δt . For $\Delta t \leq \Delta x$ the steady state is a reasonable denoising, hence we choose $\Delta t = \Delta x$ or $\Delta t = \Delta x/2$ in most of this paper. Note that this closely matches the suggested time step bound in (66) for a quantization level of $1/255$, given the other parameters utilized here, which would come out to $\Delta t \leq 1.189\Delta x$.

Figure 8 compares the energy decay against CPU time for denoising the Lenna image with PDE acceleration, Primal Dual, and Split Bregman algorithms. The noise is additive zero mean Gaussian noise with standard deviation $\sigma = 0.1$ and the images take values in the interval $[0, 1]$. We note in Figures 11 and 12 that PDE acceleration appears to yield a better quality image for the same energy level compared to primal dual.

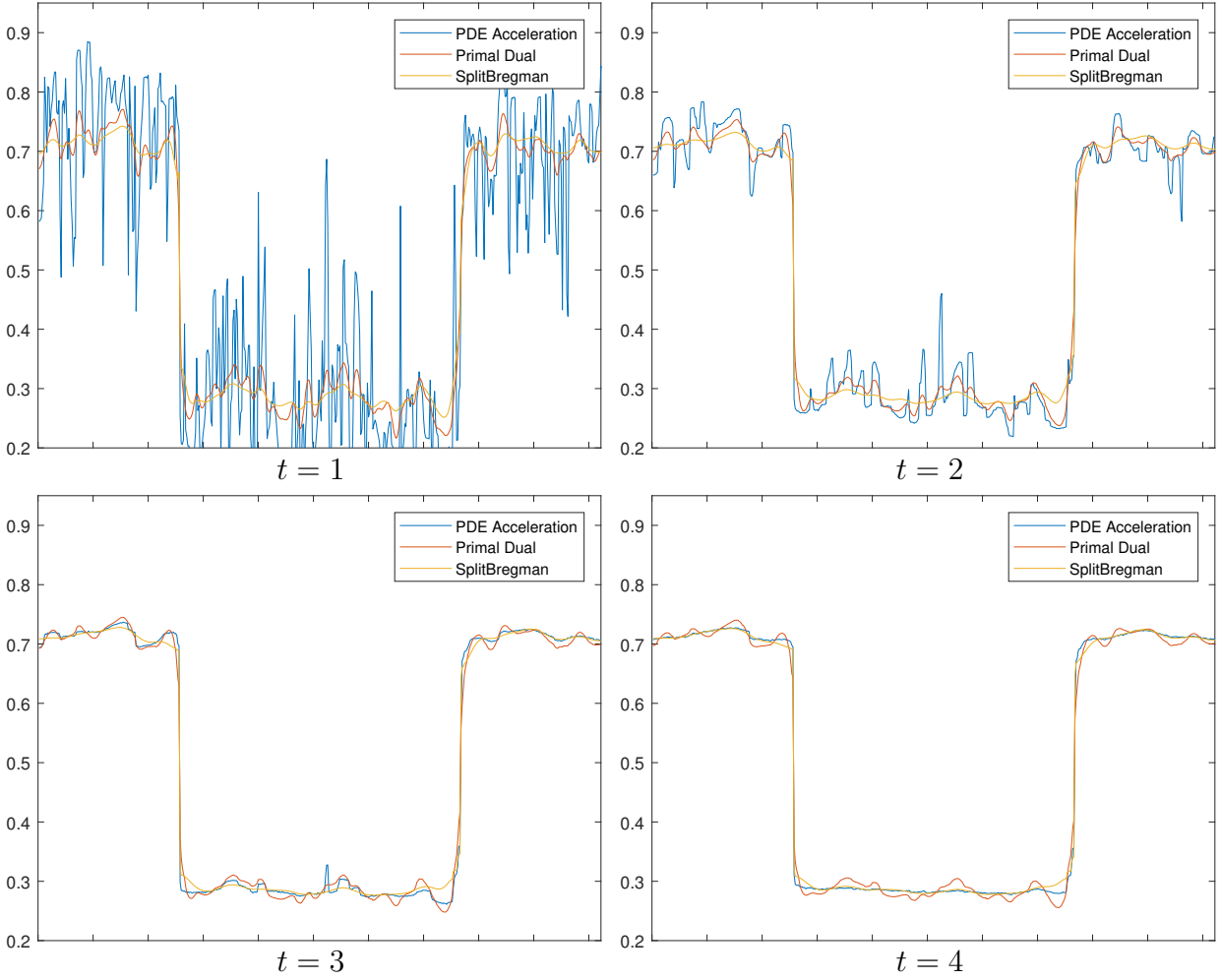


Figure 5: Comparison of PDE acceleration, Primal Dual, and Split Bregman algorithms for denoising a noisy square image. A one dimensional slice of the image is displayed at the same computation time for each algorithm.

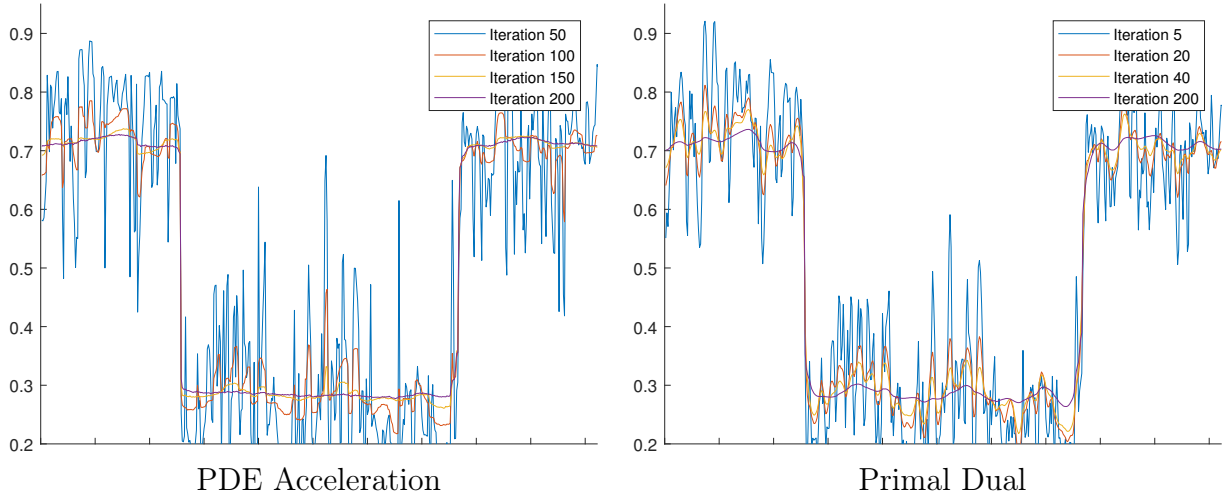


Figure 6: Comparison of flows generated by (a) PDE Acceleration and (b) Primal Dual for solving the TV restoration problem on the noisy square image. Notice the edges are better preserved in PDE acceleration earlier in the flow.

6 Conclusion

We employed the novel framework of *PDE Acceleration*, based on momentum methods such as Nesterov and Polyak’s heavy ball method, to calculus of variations problems defined for general functions on \mathbb{R}^n . The result was a very general set of *accelerated PDE’s* whose simple discretizations efficiently solve the the resulting class of optimization problems. We further analyzed their use in regularized inversion problems, where gradient descent diffusion equations get replaced by nonlinear wave equations within the framework of PDE acceleration, with far more generous discrete time step conditions.

We presented results of experiments on image processing problems including Beltrami regularized denoising and inpainting, and total variation (TV) regularized denoising and deblurring. In all cases, we can achieve state of the art results with very simple algorithms; indeed, the PDE acceleration update is a simple explicit forward Euler update of a nonlinear wave equation. Future work will focus on problems such as TV inpainting, where there is no fidelity, how to choose the damping parameter adaptively to further accelerate convergence, and applications to other problems in computer vision, such as Chan-Vese active contours [8].

References

- [1] H. Attouch, X. Goudou, and P. Redont. The heavy ball with friction method, I. The continuous dynamical system: global exploration of the local minima of a real-valued function by asymptotic analysis of a dissipative dynamical system. *Communications in Contemporary Mathematics*, 2(01):1–34, 2000.

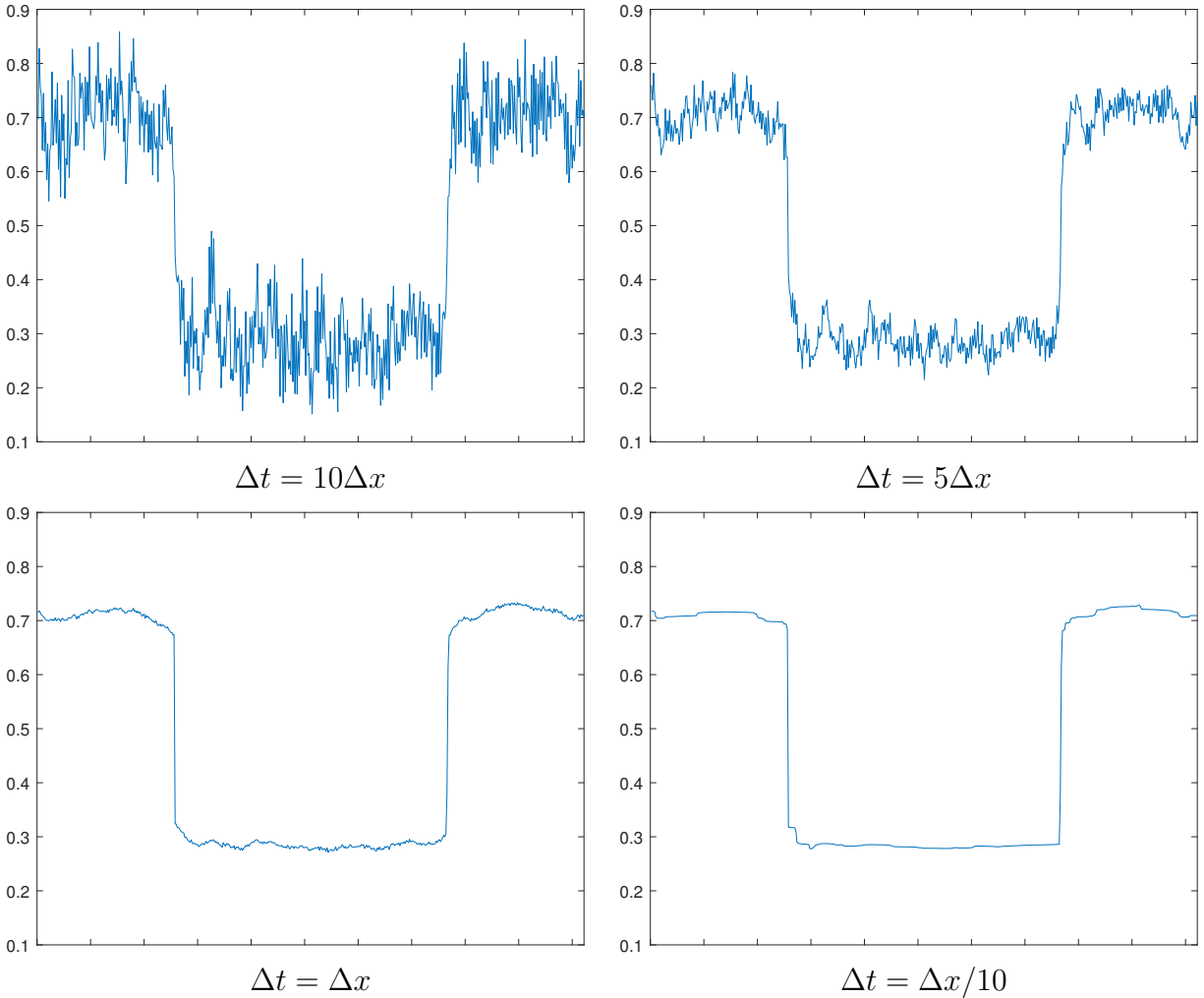


Figure 7: Comparison of steady state solutions for denoising the $2D$ noisy square for different time steps in PDE Acceleration. The scheme is stable in L^∞ for a variety of time steps though we observe $\Delta t \leq \Delta x$ is required to ensure the solution is a reasonable denoising.

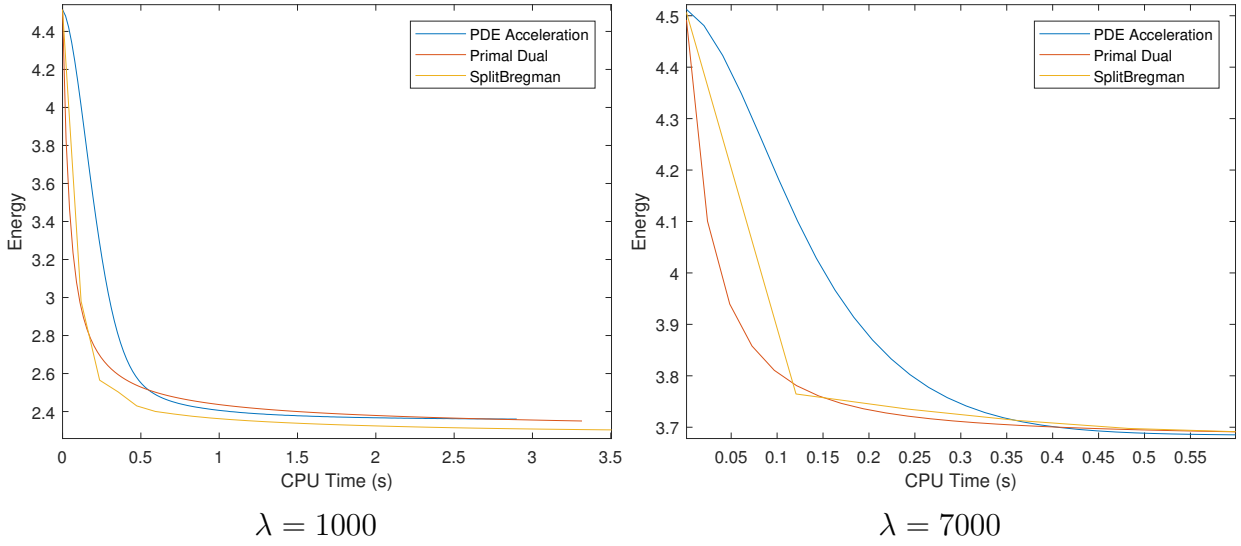


Figure 8: Comparison of logarithm of total energy versus CPU time for denoising the full 512×512 Lenna image with PDE acceleration, Primal Dual, and Split Bregman. We used $a = 6\sqrt{\lambda}$ for $\lambda = 1000$ and $a = 2\sqrt{\lambda}$ for $\lambda = 7000$.

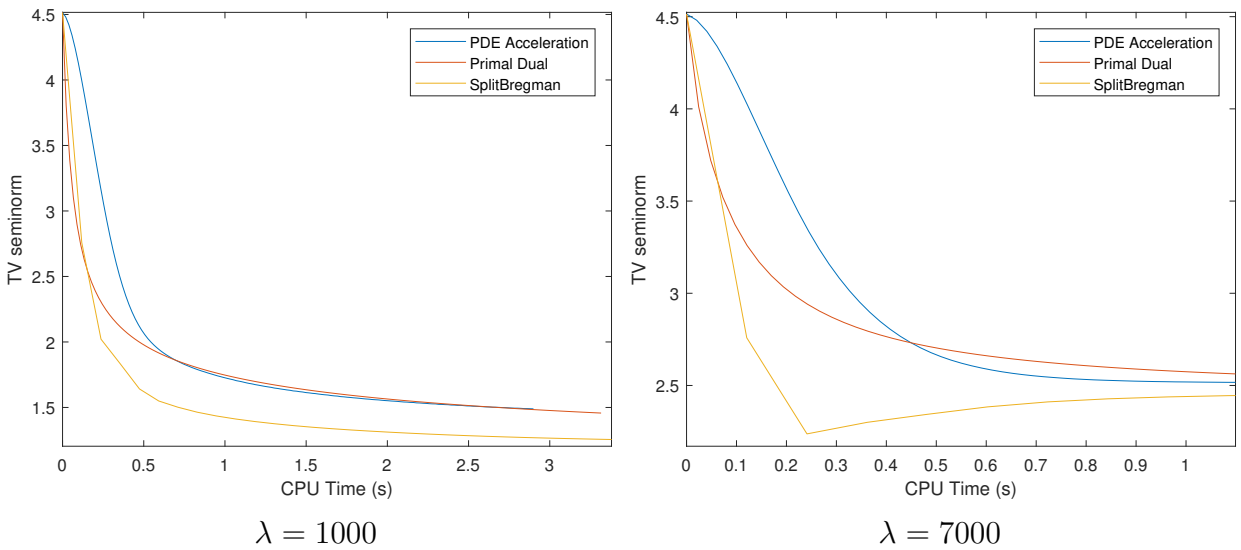


Figure 9: Comparison of logarithm of TV seminorm energy versus CPU time for denoising the full 512×512 Lenna image with PDE acceleration, Primal Dual, and Split Bregman.

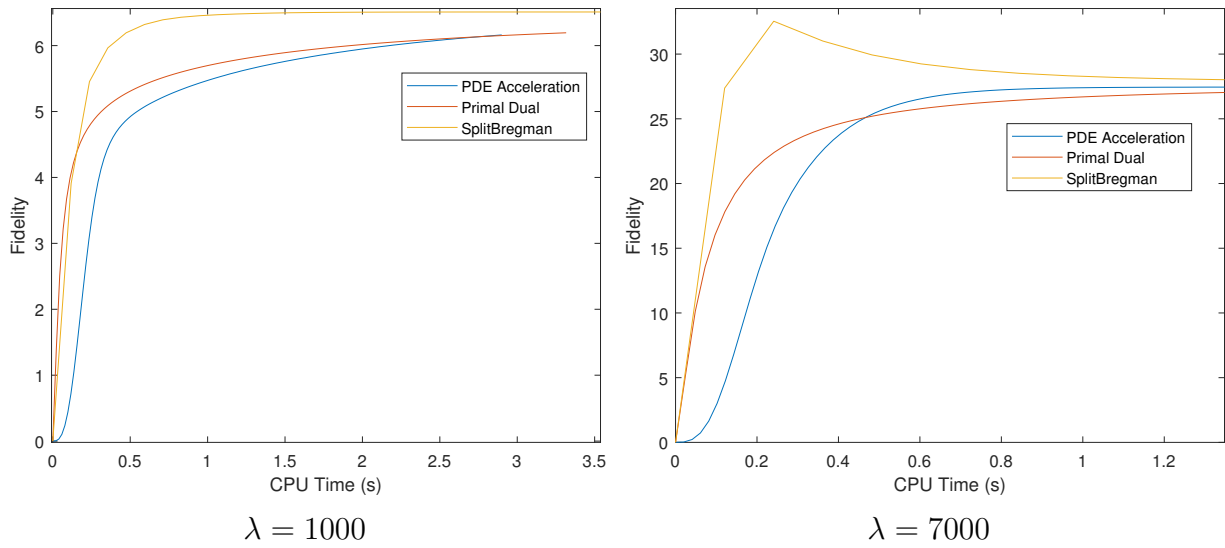


Figure 10: Comparison of fidelity energy versus CPU time for denoising the full 512×512 Lenna image with PDE acceleration, Primal Dual, and Split Bregman.

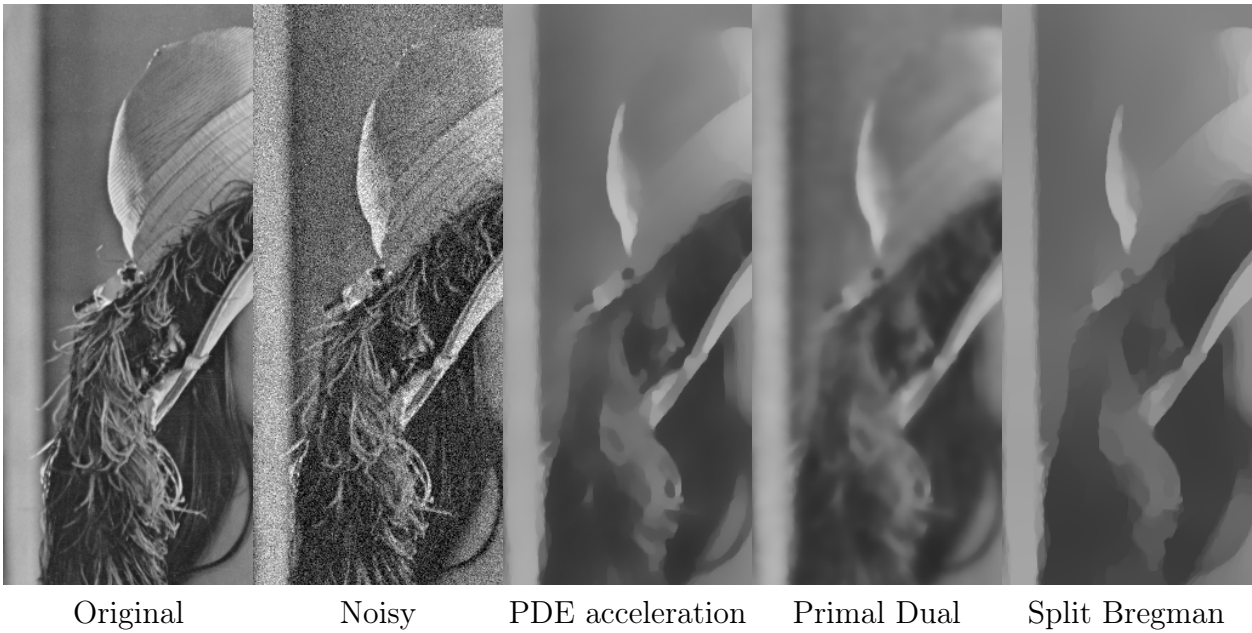


Figure 11: Comparison of PDE acceleration, Primal Dual, and Split Bregman for TV restoration of a noisy Lenna image with $\lambda = 1000$. Each algorithm was run for 150 iterations, which took 2.7 seconds for PDE acceleration, 3.3 seconds for Primal Dual, and 28 seconds for Split Bregman.

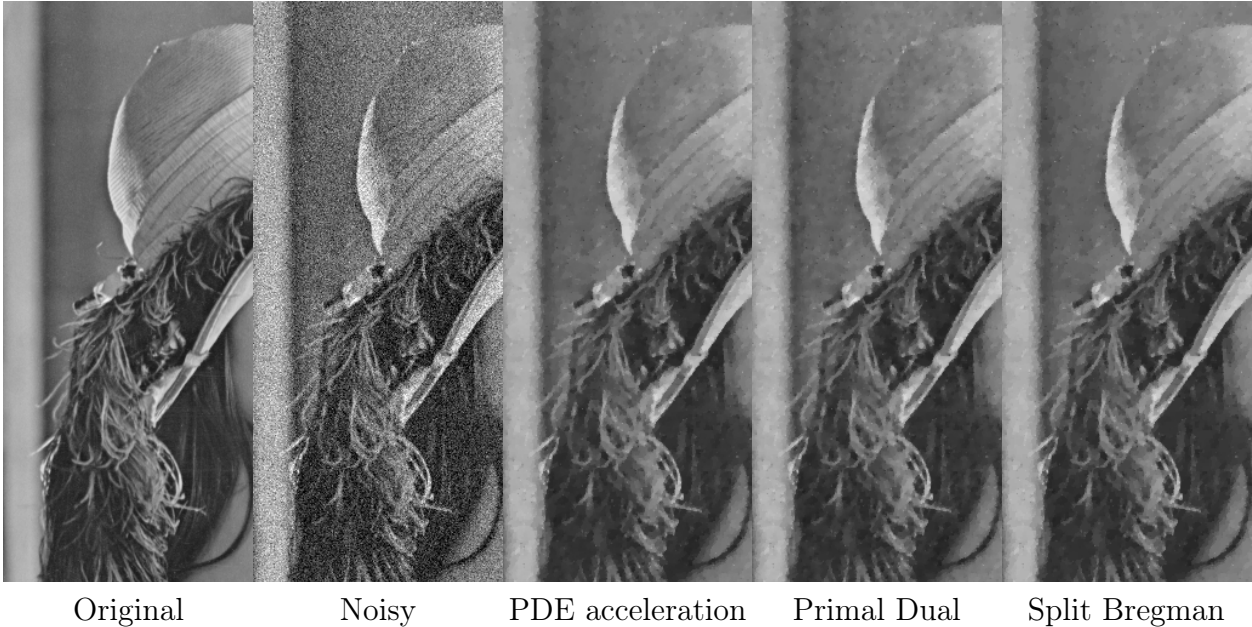


Figure 12: Comparison of PDE acceleration, Primal Dual, and Split Bregman for TV restoration of a noisy Lenna image with $\lambda = 7000$. Each algorithm was run for 50 iterations, which took 0.85 seconds for PDE acceleration, 1.12 seconds for Primal Dual, and 10.4 seconds for Split Bregman.

- [2] G. Aubert and P. Kornprobst. *Mathematical problems in image processing: partial differential equations and the calculus of variations*, volume 147. Springer Science & Business Media, 2006.
- [3] M. Bähr, M. Breuß, and R. Wunderlich. Fast explicit diffusion for long-time integration of parabolic problems. In *AIP Conference Proceedings*, volume 1863, page 410002. AIP Publishing, 2017.
- [4] L. Bottou. Large-scale machine learning with stochastic gradient descent. In *Proceedings of COMPSTAT'2010*, pages 177–186. Springer, 2010.
- [5] S. Boyd and L. Vandenberghe. *Convex optimization*. Cambridge university press, 2004.
- [6] J. Calder and A. Yezzi. An accelerated PDE framework for efficient solutions of obstacle problems. *Preprint*, 2018.
- [7] A. Chambolle and T. Pock. A first-order primal-dual algorithm for convex problems with applications to imaging. *Journal of mathematical imaging and vision*, 40(1):120–145, 2011.
- [8] T. F. Chan and L. A. Vese. Active contours without edges. *IEEE Transactions on image processing*, 10(2):266–277, 2001.

- [9] T. Goldstein and S. Osher. The split bregman method for l_1 -regularized problems. *SIAM journal on imaging sciences*, 2(2):323–343, 2009.
- [10] X. Goudou and J. Munier. The gradient and heavy ball with friction dynamical systems: The quasiconvex case. *Mathematical Programming*, 116(1-2):173–191, 2009.
- [11] S. Grewenig. FSI schemes: Fast semi-iterative solvers for PDEs and optimisation methods. In *Pattern Recognition: 38th German Conference, GCPR 2016, Hannover, Germany, September 12-15, 2016, Proceedings*, volume 9796, page 91. Springer, 2016.
- [12] D. Hafner, P. Ochs, J. Weickert, M. Reißel, and S. Grewenig. FSI schemes: Fast semi-iterative solvers for PDEs and optimisation methods. In *German Conference on Pattern Recognition*, pages 91–102. Springer, 2016.
- [13] R. Kimmel, R. Malladi, and N. Sochen. Image processing via the beltrami operator. In *Asian Conference on Computer Vision*, pages 574–581. Springer, 1998.
- [14] Y. Nesterov. A method of solving a convex programming problem with convergence rate $o(1/k^2)$. In *Soviet Mathematics Doklady*, volume 27, pages 372–376, 1983.
- [15] P. Perona and J. Malik. Scale-space and edge detection using anisotropic diffusion. *IEEE Transactions on pattern analysis and machine intelligence*, 12(7):629–639, 1990.
- [16] B. T. Polyak. Some methods of speeding up the convergence of iteration methods. *USSR Computational Mathematics and Mathematical Physics*, 4(5):1–17, 1964.
- [17] L. I. Rudin, S. Osher, and E. Fatemi. Nonlinear total variation based noise removal algorithms. *Physica D: nonlinear phenomena*, 60(1-4):259–268, 1992.
- [18] N. Sochen, R. Kimmel, and R. Malladi. A general framework for low level vision. *IEEE transactions on image processing*, 7(3):310–318, 1998.
- [19] W. Su, S. Boyd, and E. Candes. A differential equation for modeling Nesterov’s accelerated gradient method: Theory and insights. In *Advances in Neural Information Processing Systems*, pages 2510–2518, 2014.
- [20] G. Sundaramoorthi and A. Yezzi. Accelerated optimization in the PDE framework: Formulations for the manifold of diffeomorphisms. *arXiv:1804.02307*, 2018.
- [21] G. Sundaramoorthi and A. Yezzi. Variational pde’s for acceleration on manifolds and applications to diffeomorphisms. *Neural Information Processing Systems*, 2018.
- [22] I. Sutskever, J. Martens, G. Dahl, and G. Hinton. On the importance of initialization and momentum in deep learning. In *International conference on machine learning*, pages 1139–1147, 2013.

- [23] C. Ward, N. Whitaker, I. Kevrekidis, and P. Kevrekidis. A toolkit for steady states of nonlinear wave equations: Continuous time Nesterov and exponential time differencing schemes. *arXiv:1710.05047*, 2017.
- [24] J. Weickert, S. Grewenig, C. Schroers, and A. Bruhn. Cyclic schemes for PDE-based image analysis. *International Journal of Computer Vision*, 118(3):275–299, 2016.
- [25] A. Wibisono, A. C. Wilson, and M. I. Jordan. A variational perspective on accelerated methods in optimization. *Proceedings of the National Academy of Sciences*, 113(47):E7351–E7358, 2016.
- [26] A. Yezzi and G. Sundaramoorthi. Accelerated optimization in the PDE framework: Formulations for the active contour case. *arXiv:1711.09867*, 2017.
- [27] D. Zosso and A. Bustin. A primal-dual projected gradient algorithm for efficient beltrami regularization. *Computer Vision and Image Understanding*, pages 14–52, 2014.